© 2020. Published by The Company of Biologists Ltd | Development (2020) 147, dev189506. doi:10.1242/dev.189506

RESEARCH ARTICLE

The Fgf8 subfamily (Fgf8, Fgf17 and Fgf18) is required for closure of the embryonic ventral body wall

Michael Boylan[1], Matthew J. Anderson[1], David M. Ornitz[2] and Mark Lewandoski[1,*]

ABSTRACT

The closure of the embryonic ventral body wall in amniotes is an important morphogenetic event and is essential for life. Defects in human ventral wall closure are a major class of birth defect and a significant health burden. Despite this, very little is understood about how the ventral body wall is formed. Here, we show that fibroblast growth factor (FGF) ligands FGF8, FGF17 and FGF18 are essential for this process. Conditional mouse mutants for these genes display subtle migratory defects in the abdominal muscles of the ventral body wall and an enlarged umbilical ring, through which the internal organs are extruded. By refining where and when these genes are required using different Cre lines, we show that *Fgf8* and *Fgf17* are required in the presomitic mesoderm, whereas *Fgf18* is required in the somites. This study identifies complex and multifactorial origins of ventral wall defects and has important implications for understanding their origins during embryonic development.

KEY WORDS: Omphalocele, Fibroblast growth factor, Ventral body wall

INTRODUCTION

Embryonic ventral wall (VW) defects are a class of congenital abnormality and are relatively frequently encountered in the clinic. Omphalocele is a VW defect where the viscera are herniated through an enlarged umbilical ring. Usually, the organs remain covered by the amnion (Williams, 2008). Severity can range from only a portion of liver being herniated to the extrusion of multiple organs. Omphalocele is frequently co-morbid with other defects, especially cardiac defects, pulmonary hypertension and chromosomal abnormalities (Corey et al., 2014; Marshall et al., 2015), and these contribute to the high perinatal mortality rate. Omphalocele is sometimes confused with another VW defect, gastroschisis, and this confusion has been noted in the literature (Carnaghan et al., 2013; Williams, 2008). In omphalocele, the defect is centered on the umbilical ring and the viscera are contained within the amniotic membrane unless the membrane has ruptured (Brewer and Williams, 2004a). In gastroschisis the defect is dextral to the umbilical ring, usually only loops of midgut are herniated, and the defect is never covered by a membrane (Brewer and Williams, 2004a).

Despite its medical relevance, VW closure is poorly understood. The VW has two components, the primary and secondary VW, both derived from the embryonic mesoderm emerging from the primitive streak. The primary VW is the initial covering for the ventral surface, and, in the mouse, is formed at embryonic day (E) 9.5 by the midline fusion of the left and right halves of the lateral plate mesoderm (LPM). At around E11.0, muscle, tendon and cartilage progenitors from the somites migrate ventrolaterally (Nichol et al., 2012); these will form the abdominal muscles, connective tissues and ribs, respectively, that comprise the secondary VW. Migration is complete by E14.5, but the midgut, within the physiological hernia, still protrudes from the embryo through the umbilical ring, where the umbilical vessels connect into the embryo. The midgut returns to the abdomen by E16.5. In human omphalocele, migration of abdominal wall muscles appears immature and disorganized (Nichol et al., 2012), leading to the hypothesis that defects in muscle migration causes omphalocele in both mice and humans. However, many mouse models of muscle defects have been described that do not report VW defects (Grifone et al., 2005; Rudnicki et al., 1993; Tremblay et al., 1998), making the causative relationship between secondary VW migration and omphalocele unclear.

The fibroblast growth factor (FGF) pathway is one of the cardinal cell signaling pathways in embryology, with 18 secreted signaling ligands grouped into seven subfamilies based on their sequence homology (Ornitz and Itoh, 2015). *Fgf8* is expressed early in embryogenesis (Crossley and Martin, 1995) and is essential for the morphogenesis of many tissues including the kidneys (Perantoni et al., 2005), limbs (Crossley et al., 1996; Lewandoski et al., 2000) and others, and is also essential for gastrulation (Sun et al., 1999). Based on amino acid sequence similarity, there are two other members of the *Fgf8* subfamily, *Fgf17* and *Fgf18*, with unique expression patterns during embryonic development (Maruoka et al., 1998; Xu et al., 1999). *Fgf17* plays a role in brain development (Cholfin and Rubenstein, 2007; Xu et al., 1999), and although *Fgf17* null mice are viable, they exhibit subtle behavioral abnormalities (Scearce-Levie et al., 2008). *Fgf18* is important in regulating chondrogenesis and osteogenesis (Hung et al., 2016; Liu et al., 2007, 2002; Ohbayashi et al., 2002). *Fgf8* expression in the presomitic mesoderm (PSM) plays a role in the wavefront of somitogenesis, an activity that prevents differentiation of this tissue (Dubrulle and Pourquié, 2004; Naiche et al., 2011). *Fgf17* and *Fgf18* are also expressed in the PSM (Maruoka et al., 1998), but a functional PSM role is unknown for these two genes. Owing to their ability to genetically compensate for one another, FGF ligand requirements in any morphogenetic processes can be obscured until multiple ligands are inactivated (Naiche et al., 2011). We decided to search for genetic interactions between the members of the *Fgf8* subfamily, *Fgf8*, *Fgf17* and *Fgf18*, within the PSM. We found that

[1]Cancer and Developmental Biology Lab, National Cancer Institute, National Institutes of Health, Frederick, MD 21702, USA. [2]Department of Developmental Biology, Washington University School of Medicine, Saint Louis, MO 63110, USA.

*Author for correspondence (lewandom@nih.gov)

M.L., 0000-0002-1066-3735

Handling Editor: Sally Dunwoodie
Received 17 February 2020; Accepted 28 August 2020

Development (2020) 147, dev189506. doi:10.1242/dev.189506

when all three genes are conditionally inactivated, we recovered embryos with omphalocele.

Other signaling pathways have been implicated in controlling VW morphogenesis including the Hedgehog (Matsumaru et al., 2014), TGFβ (Aldeiri et al., 2017), PCP (Murdoch et al., 2014) and canonical Wnt (Zhang et al., 2014) pathways. Inactivating some downstream components of the FGF pathway has been shown to result in omphalocele. Inactivating of one copy of *Fgfr1* and both copies of *Fgfr2* using a global inducible Cre causes omphalocele (Nichol et al., 2011). Similarly, inactivating *Mek1* (also known as *Map2k1*) in a *Mek2* (*Map2k2*) null background with a mesenchyme-specific Cre resulted in omphalocele (Boucherat et al., 2014). Here, we investigate the genetic interaction between different members of the *Fgf8* subfamily and examine their roles in VW morphogenesis. By using different tissue-specific Cre recombinase mouse lines, we demonstrate that the requirement for these genes in VW morphogenesis is in the PSM and somites. This is the first evidence connecting a loss of FGF ligand function to VW defects.

RESULTS

The Fgf8 subfamily is expressed in progenitors of the primary and secondary body wall

We first examined the expression patterns of *Fgf8* (Fig. 1A-E), *Fgf17* (Fig. 1F-J) and *Fgf18* (Fig. 1K-O) from E7.75 through to E11.5 using RNA whole-mount *in situ* hybridization reaction (WISH). We developed the chromogenic stain for an extended period of time to reveal domains of low gene expression. Both *Fgf8* and *Fgf17* were expressed in the primitive streak, tailbud and the PSM (Fig. 1A-J). *Fgf8* (Fig. 1C-E) was expressed in the myotome of the somites, whereas *Fgf18* (Fig. 1K-O) was expressed more broadly in somites. In addition to these observations, which replicate previously published expression patterns (Crossley and Martin, 1995; Hagan et al., 2019; Maruoka et al., 1998; Stolte et al., 2002), we report previously undescribed expression patterns for *Fgf8* and *Fgf18*. At E11.5, *Fgf8* was weakly expressed in the myotome in the interlimb region, as well as in the condensing portions of the limb (Fig. 1E). *Fgf18* was expressed in the neuroepithelium of the tailbud from E8.5 through E10.5 (Fig. 1L-O) and in the dermomyotome at E11.5 (Fig. 1O).

Fgf8 and *Fgf17* are expressed in the primitive streak and PSM, which gives rise to the LPM and ultimately to the primary VW; the PSM also forms the somites, which generate the secondary VW. *Fgf8* and *Fgf18* are also expressed in the somites themselves. These experiments demonstrate that these Fgfs are expressed in the progenitors of the embryonic structures that will close the VW. The data in Fig. 1 indicate that there is either no or very low expression of these ligand genes in the primary VW or secondary VW layers themselves. To address this directly, we generated mRNA E11.5 *in situ* hybridization chain reaction (HCR) data for each of the three FGF ligand genes (Fig. S1). These analyses confirmed our

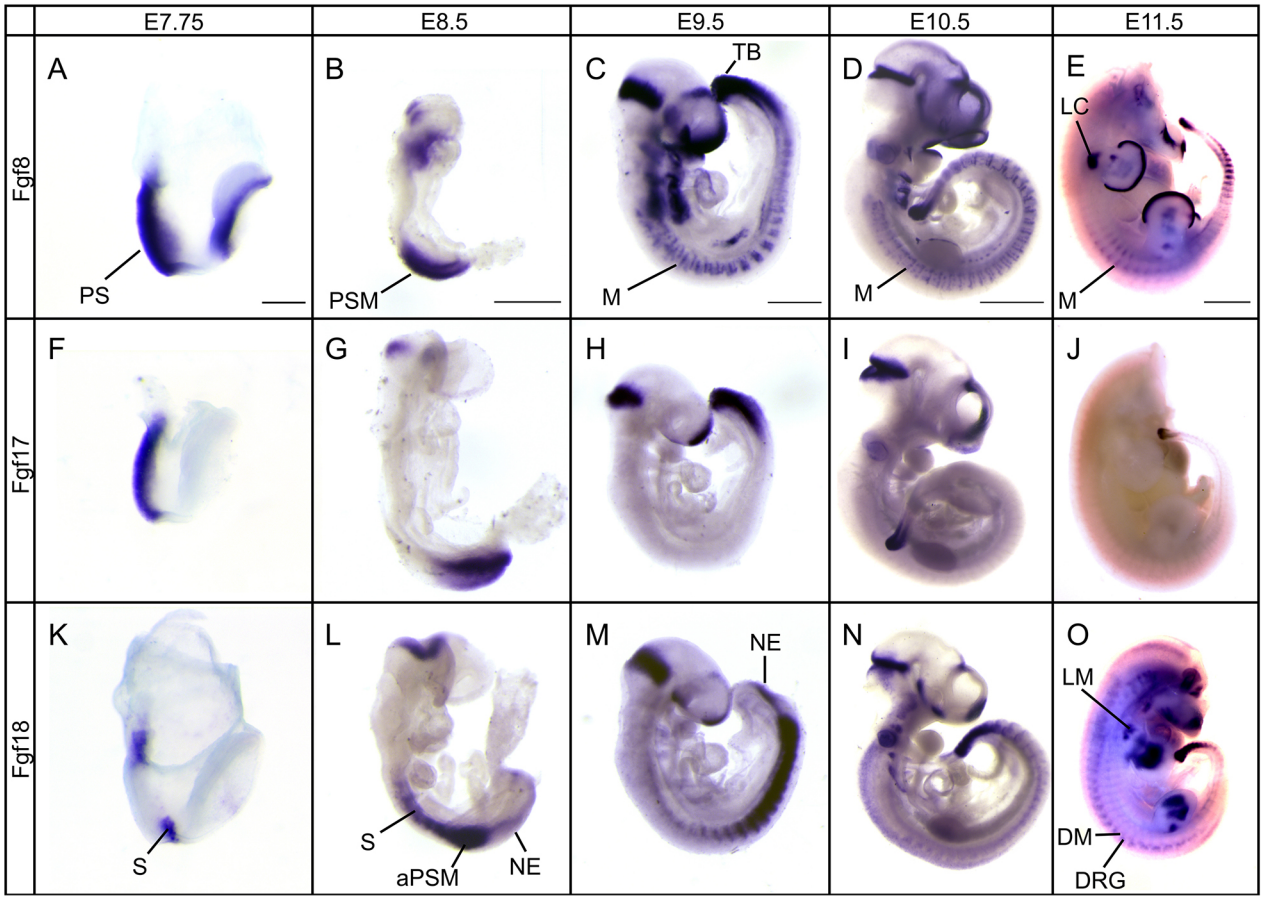

Fig. 1. Members of the *Fgf8* subfamily are expressed in multiple overlapping domains. (A-E) Expression pattern of *Fgf8* from E7.75 to E11.5. (F-J) Expression pattern of *Fgf17* from E7.75 to E11.5. (K-O) Expression pattern of *Fgf18* from E7.75 to E11.5. E11.5 embryos were decapitated before WISH to reduce probe trapping. All three genes are expressed in and around the PSM, and *Fgf8* and *Fgf18* are expressed in the somites and the dermomyotome and myotome. aPSM, anterior presomitic mesoderm; DM, dermomyotome; DRG, dorsal root ganglion; LC, limb bud condensation; LM, limb muscle; M, myotome; NE, neuroepithelium; PS, primitive streak; PSM, presomitic mesoderm; S, somite; TB, tail bud. Scale bars: 250 µm (A); 500 µm (B,C); 1 mm (D,E).

Development (2020) 147, dev189506. doi:10.1242/dev.189506

observation that there is little to no detectable expression within the VW itself.

The Fgf8 subfamily is required to close the ventral body wall

Inactivation of *Fgf8* in the nascent mesoderm, emerging from the primitive streak via Tg(T-cre)1Lwd (hereafter 'TCre') transgenic activity, demonstrated its role in nephrogenesis (Perantoni et al., 2005) and the male urogenital tract (Kitagaki et al., 2011). Inactivation of *Fgf8* simultaneously with *Fgf4* using TCre showed that these FGFs redundantly maintain the PSM in an undifferentiated state (Naiche et al., 2011). Therefore, we asked whether there were redundant roles for the *Fgf8* subfamily in the nascent mesoderm and its derivatives. To address this, we conditionally inactivated *Fgf8* and *Fgf18* in the primitive steak using TCre on an *Fgf17* null background (Table S1). We confirmed that TCre recombines in the primitive streak and thus throughout most of the mesoderm by breeding TCre males to *Gt(ROSA)26Sor*$^{tm4(ACTB\text{-}tdTomato,\text{-}EGFP)Luo}$/J (hereafter '*mTmG*') reporter females (Muzumdar et al., 2007) (Fig. S2A). We confirmed that both floxed genes were recombined using WISH analysis with riboprobes directed against the deleted region of each gene and observed that expression of *Fgf8* and *Fgf18* was abolished in tissues recombined by Cre recombinase (Fig. S2B-E).

At E18.5 TCre;*Fgf8*$^{f/+}$;*Fgf17*$^{\Delta/\Delta}$;*Fgf18*$^{f/+}$ offspring (hereafter 'controls') were healthy and viable with no obvious abnormal phenotype (Fig. 2A). However, when we generated TCre;*Fgf8*$^{f/\Delta}$;*Fgf17*$^{\Delta/\Delta}$;*Fgf18*$^{f/\Delta}$ littermates (hereafter 'triple mutants') we found that these embryos frequently had omphalocele (Fig. 2B), with 71% penetrance (Fig. 2G). This failure to close the ventral body was always abdominal and never affected the thoracic body wall. TCre;*Fgf8*$^{f/\Delta}$;*Fgf17*$^{\Delta/\Delta}$;*Fgf18*$^{f/+}$ offspring (Fig. 2C) occasionally had omphalocele (Fig. 2C′,G) but otherwise resembled TCre;*Fgf8*$^{f/\Delta}$ animals (Kitagaki et al., 2011; Perantoni et al., 2005). TCre;*Fgf8*$^{f/+}$;*Fgf17*$^{\Delta/\Delta}$;*Fgf18*$^{f/\Delta}$ embryos (Fig. 2D) also occasionally presented with omphalocele (Fig. 2D′,G), but otherwise displayed no additional phenotype beyond the kyphosis and other skeletal defects already reported for TCre;*Fgf18*$^{f/\Delta}$ animals (Hagan et al., 2019) (Fig. S3C,G). We observed that embryos were present in non-Mendelian ratios, with triple mutants appearing underrepresented (P<0.02, two-tailed Chi^2 test) compared with controls. As described below, this is likely because a subset of these mutants failed to undergo proper yolk sac development.

In triple mutant embryos the omphalocele ranged in severity, from only a portion of the liver being herniated, to most of the liver as well as the large and small intestine and the stomach being herniated. The amnion around the hernia indicated that the defect was omphalocele, not gastroschisis. Sections revealed that there were no gross morphological defects in the abdominal muscles at E18.5 in triple mutants (n=4), with all the muscle layers present and morphologically normal (Fig. 2E,F). The skeletal defects attributable to a loss of *Fgf18* (Hagan et al., 2019; Hung et al., 2016; Liu et al., 2007, 2002; Ohbayashi et al., 2002) in the triple

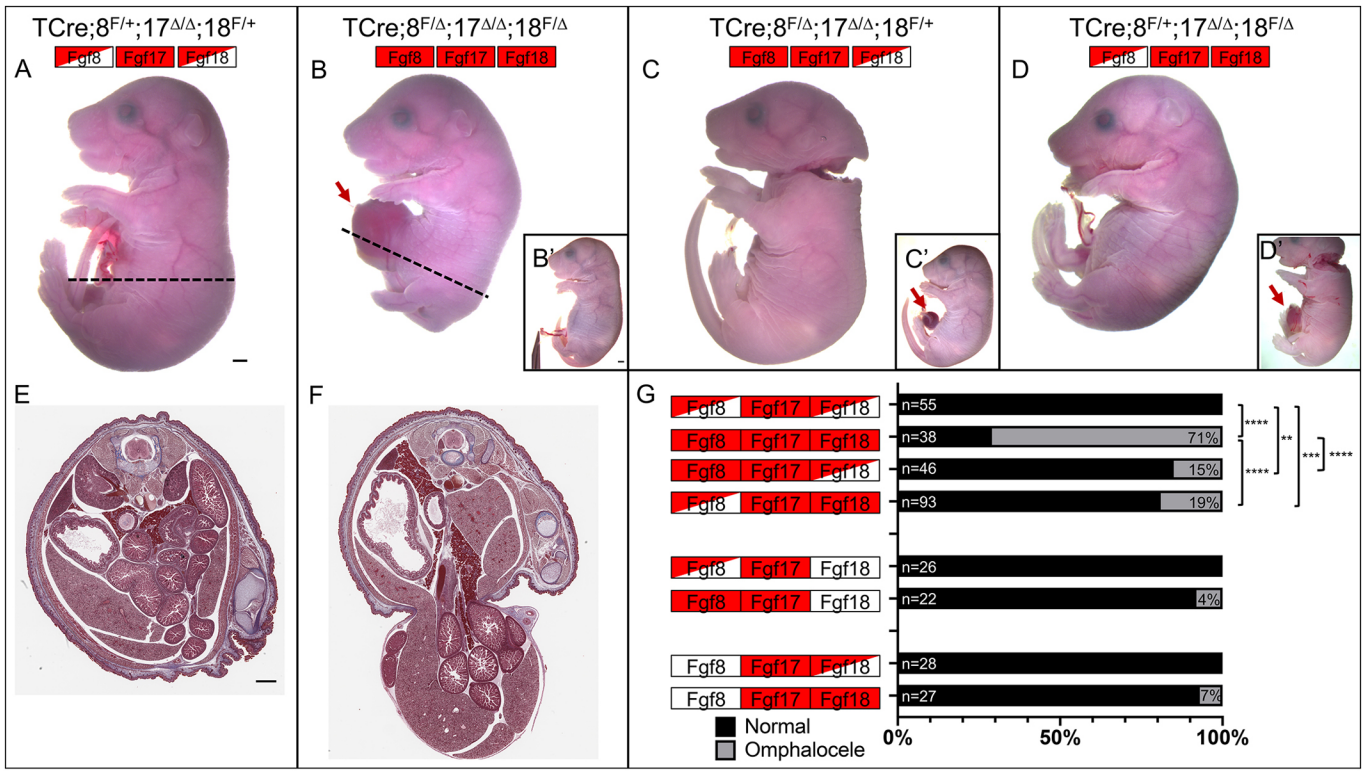

Fig. 2. E18.5 *Fgf8* subfamily triple mutants have omphalocele. (A) Control embryos appear phenotypically normal. (B) Most triple mutants have omphalocele (arrow), though a subset do not (B′). (C) TCre;*Fgf8*$^{fl\Delta}$,*17*$^{\Delta/\Delta}$,*18*$^{fl/+}$ embryos usually appear phenotypically normal, but a subset have omphalocele (C′). (D) TCre;*Fgf8*$^{fl/+}$,*17*$^{\Delta/\Delta}$,*18*$^{fl\Delta}$ offspring have kyphosis and bowed limbs; a minority of embryos also have omphalocele (D′). (E,F) transverse sections of control (E) and triple mutant (F) embryos stained with Masson's trichrome. The axial level of the section is indicated by the dashed line in A and B. The omphalocele is within an amniotic sac, and all five layers of muscle are present, albeit thinner (n=4). (G) Graphical representation of the incidence of omphalocele showing the percentage of embryos with and without omphalocele. The total number of embryos is to the left of the bars and the percentage of embryos with omphalocele is on the right. Significance was determined using a two-tailed Fisher's exact test. **P<0.01, ***P<0.001, ****P<0.0001. Boxes indicate genotype: an empty box indicates two wild-type alleles; a half red, half empty box indicates one mutant and one wild-type allele; a fully red box indicates two mutant alleles. Scale bars: 1 mm.

Development (2020) 147, dev189506. doi:10.1242/dev.189506

mutants were more severe than in TCre;*Fgf8*$^{f/+}$;*Fgf17*$^{Δ/Δ}$;*Fgf18*$^{f/Δ}$ embryos (Fig. S3D,H). In triple mutants the kyphosis was more pronounced and the ribs more bowed than in TCre;*Fgf8*$^{f/+}$;*Fgf17*$^{Δ/Δ}$;*Fgf18*$^{f/Δ}$ embryos (compare Fig. S3C,G with D,H). Although the sternum appeared kinked because of the rib abnormalities, it had fused correctly (Fig. S3D′). No other abnormalities that are often associated with VW defects, such as genitourinary deformities (Matsumaru et al., 2014) or diaphragmatic hernia (Stoll et al., 2008), were observed.

We then proceeded to test the dosage requirements for each gene in recovering omphalocele by performing a genetic series in which different members of the *Fgf8* subfamily are inactivated in different combinations. We observed that in the triple mutants, the recovery rate of omphalocele was 71% (Fig. 2G); when both copies of *Fgf17* are intact in a TCre;*Fgf8*$^{f/Δ-}$;*Fgf18*$^{f/Δ}$ background this rate was reduced to 52% (Fig. S4), suggesting a role for *Fgf17*, although this reduction was not significant (P=0.1733, two-tailed Fisher's exact test). To analyze the role of *Fgf17* further we considered double mutants in which *Fgf17* was inactivated along with either *Fgf8* or *Fgf18*. In such mutants (TCre;*Fgf8*$^{f/Δ}$;*Fgf17*$^{Δ/Δ}$;*Fgf18*$^{+/+}$ and TCre;*Fgf8*$^{+/+}$;*Fgf17*$^{Δ/Δ}$;*Fgf18*$^{f/Δ}$) the incidence of omphalocele was 4% and 7%, respectively (Fig. 2G). When only *Fgf8* (n=18) or *Fgf18* (n=30) were inactivated via TCre-mediated recombination, omphalocele never occurred, demonstrating a small but real effect from the loss of *Fgf17*. Having established that all three genes play a role, we continued the analysis in an *Fgf17* null background.

Omphalocele occurs between E12.5 and E13.5 and is associated with defects in the structures of the body wall

To determine when omphalocele occurs, we performed timed dissections at E12.5 and E13.5. At E13.5, the phenotype was fully evident (Fig. 3A-C), with the rate of occurrence equivalent to E18.5 (76% versus 71%, respectively). At this developmental stage, the only morphological evidence of omphalocele was the aberrant presence of liver in the physiological hernia (Fig. 3B, red arrow). Embryos were recorded as positive for omphalocele if any piece of liver was present. If these small extrusions of liver into the physiological hernia returned to the abdomen, the incidence of omphalocele would be overcounted at E13.5 compared with E18.5, which could account for the apparent increase in omphalocele at E13.5 in both controls and in TCre;*Fgf8*$^{f/+}$;*Fgf17*$^{Δ/Δ}$;*Fgf18*$^{f/Δ}$ embryos (compare Fig. 2G with Fig. 3C). At E12.5, omphalocele was infrequently observed (9%) in triple mutants, and never observed in any other genotype (Fig. 3D). From this we concluded that omphalocele has not yet occurred at E12.5 in the vast majority of embryos.

We also examined earlier embryonic stages. At E10.5 in TCre;*Fgf8*$^{f/Δ}$;*Fgf17*$^{Δ/Δ}$;*Fgf18*$^{f/+}$ embryos and in triple mutants, a

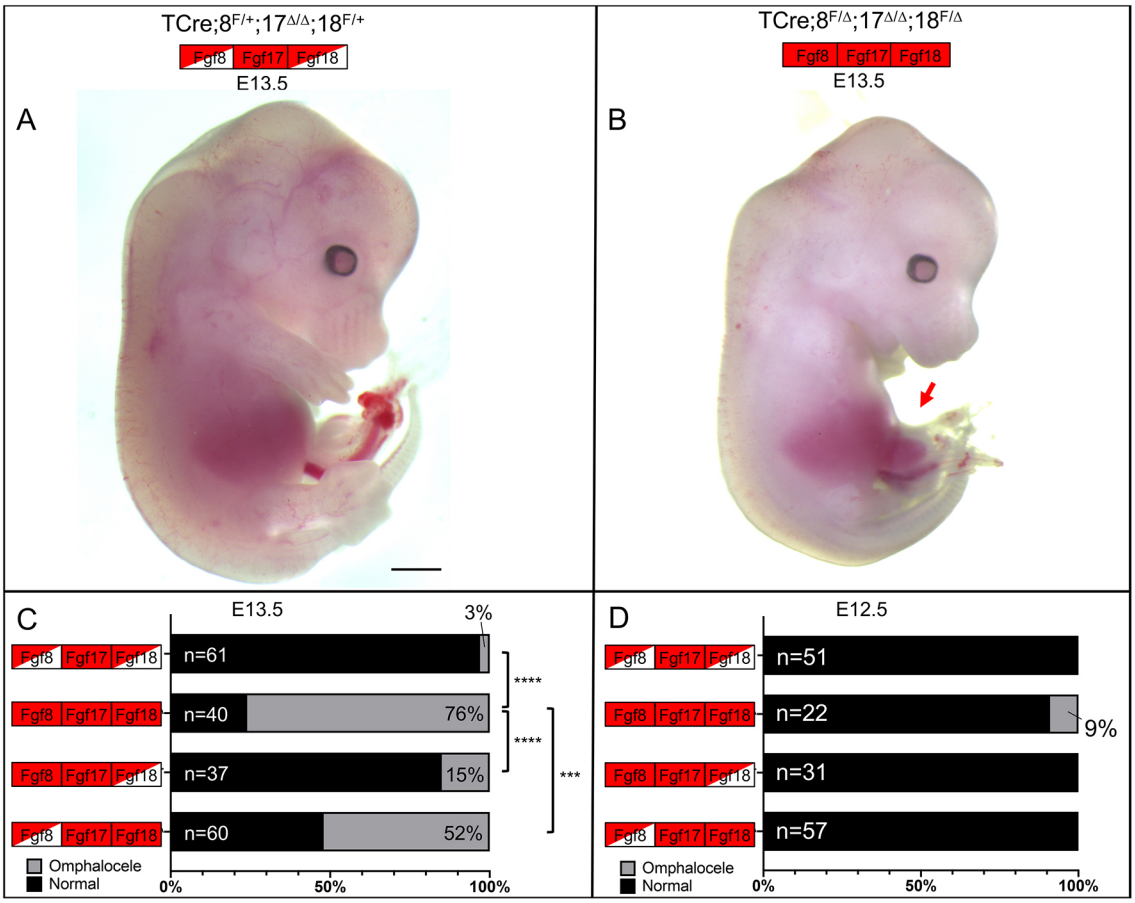

Fig. 3. The omphalocele phenotype in triple mutants is evident at E13.5. (A) E13.5 control embryo. (B) E13.5 triple mutant embryo with an abnormal inclusion of liver in the physiological hernia (arrow), indicating omphalocele. (C,D) Graphical representation of the incidence of omphalocele at E13.5 (C) and E12.5 (D) showing the percentage of embryos with and without omphalocele. The total number of embryos is to the left of the bars and the percentage of embryos with omphalocele is on the right. Significance was determined using a two-tailed Fisher's exact test. ***P<0.001, ****P<0.0001. Boxes indicate genotype; see Fig. 2 legend for key. Scale bar: 1 mm.

Development (2020) 147, dev189506. doi:10.1242/dev.189506

significant subset had failed to undergo proper yolk sac development (Fig. S5A,B). The incidence of defects at E10.5 trended higher in triple mutant embryos compared with TCre;*Fgf8*$^{f/\Delta}$;*Fgf17*$^{\Delta/\Delta}$;*Fgf18*$^{f/+}$ embryos (Fig. S5C), suggesting that the loss of *Fgf18* increases the penetrance of the yolk sac defects. This explains why there are fewer embryos of these genotypes at E18.5, as some of these embryos would have died *in utero* (Fig. 2G).

Having established that the window in which VW closure fails is between E12.5 and E13.5, we undertook a histological analysis and examined the primary VW and secondary VW at E13.5 and E12.5. Transverse sections through the abdomen at E13.5 showed that the secondary VW had migrated most of the way to the umbilical ring in both controls and triple mutants (Fig. 4A,B). We could also observe that in mutants the amniotic sac also contained a portion of the liver, and sometimes other organs too (Fig. 4B, red arrow). We measured the length of the embryonic flank from the dorsal muscle mass to the umbilical ring (Fig. 4E); the flank contains both the primary VW and secondary VW (Fig. 4F). All three mutant genotypes had significantly shorter flanks compared with controls, but triple mutants were the most severely affected. We measured the secondary VW and the primary VW individually (dashed yellow and red lines, respectively, in Fig. 4C,D). We found that although the length of the primary VW was unchanged (Fig. 4G), the primary VW was thinner in triple mutants (Fig. S6A-E). The secondary VW was much shorter in triple mutants when compared with any other genotype (Fig. 4H). We also saw that TCre;*Fgf8*$^{f/\Delta}$;*Fgf17*$^{\Delta/\Delta}$;*Fgf18*$^{f/+}$ and TCre;*Fgf8*$^{f/+}$;*Fgf17*$^{\Delta/\Delta}$;*Fgf18*$^{f/\Delta}$ embryos had a shorter secondary VW than controls, although in TCre;*Fgf8*$^{f/+}$;*Fgf17*$^{\Delta/\Delta}$;*Fgf18*$^{f/\Delta}$ embryos this was just below significance (P=0.054).

We then performed the same analysis at E12.5, before omphalocele occurs in most mutants (Fig. 3D). We examined transverse sections and saw that the secondary VW had migrated about halfway to the umbilical ring in controls (Fig. 5A,C) and in triple mutants (Fig. 5B,D); we observed no liver in the physiological hernia in mutants. When we measured the diameter of the umbilical ring, we found that in triple mutants the umbilical ring was

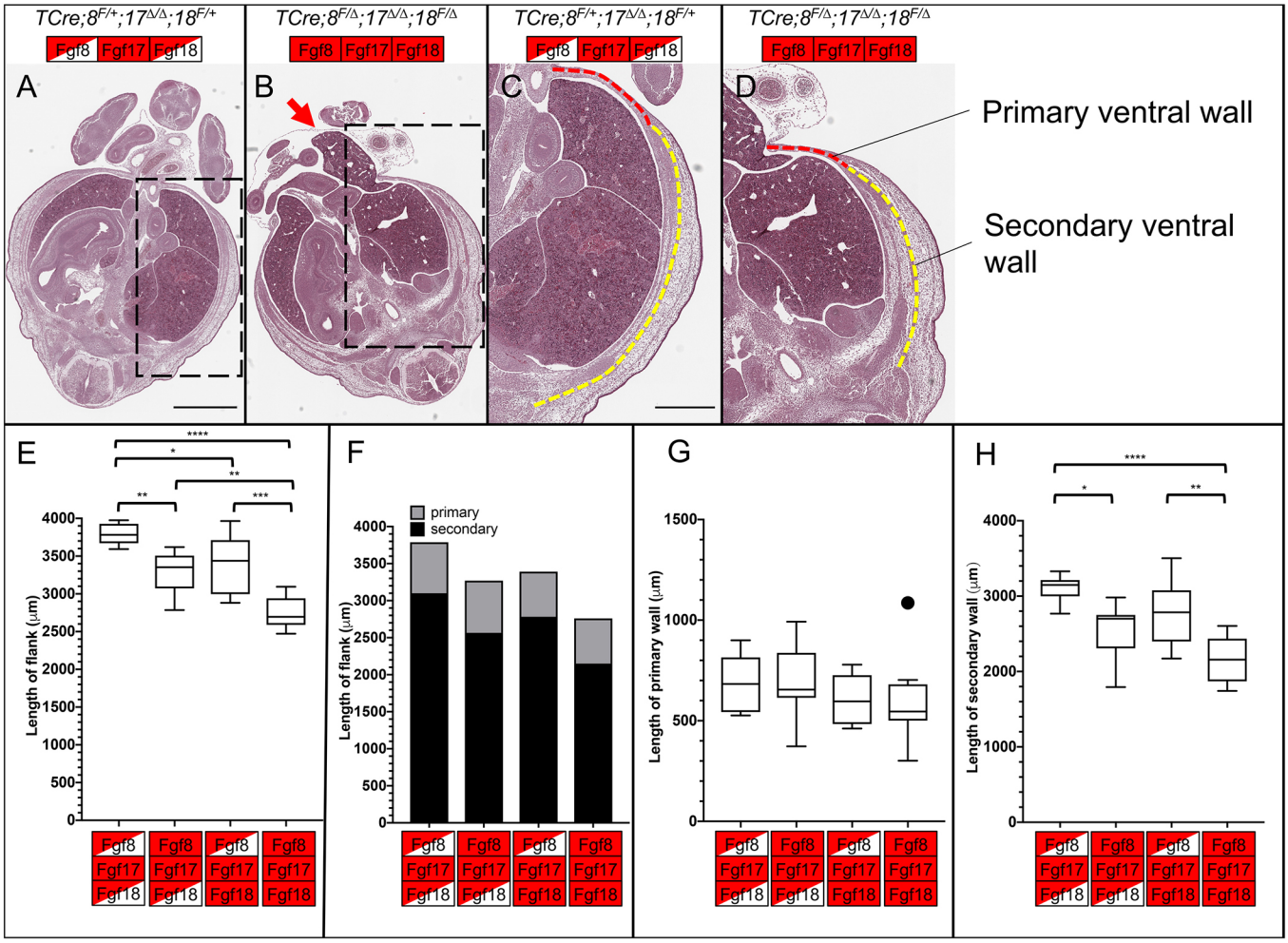

Fig. 4. Morphometric analysis of sections at E13.5 reveals changes in the secondary VW of *Fgf8* subfamily mutants. (A,B) Transverse section of E13.5 control (A) and triple mutant (B) at the interlimb region. Note the inclusion of liver in the physiological hernia of the triple mutant (arrow). (C,D) Enlargement of boxed regions of A (C) and B (D) showing the primary (red dashed line) and secondary (yellow dashed line) VWs. (E-H) Morphometric measurements of transverse sections of the indicated genotype. (E) Tukey box-plot of the primary and secondary VW added together, forming the whole flank of the embryo. (F) Bar chart of the mean length of the primary (gray) and secondary (black) VW. (G) Tukey box-plot of the primary VW, showing no differences between any genotype. (H) Tukey box-plot of the secondary VW, showing a highly significant reduction in triple mutants. Box plots show median values (middle bars) and first to third interquartile ranges (boxes); whiskers indicate 1.5× the interquartile ranges; outliers in box-plots are plotted individually. Control n=8; TCre;*Fgf8*$^{f/\Delta}$,*17*$^{\Delta/\Delta}$,*18*$^{f/+}$ n=7; TCre;*Fgf8*$^{f/+}$,*17*$^{\Delta/\Delta}$,*18*$^{f/\Delta}$ n=8; triple mutant n=9. Significance was determined using a post-hoc Tukey-Kramer test. *P<0.05, **P<0.01, ***P<0.001, ****P<0.0001. Boxes indicate genotype, see Fig. 2 for key. Scale bars: 1 mm (A); 500 µm (C).

Development (2020) 147, dev189506. doi:10.1242/dev.189506

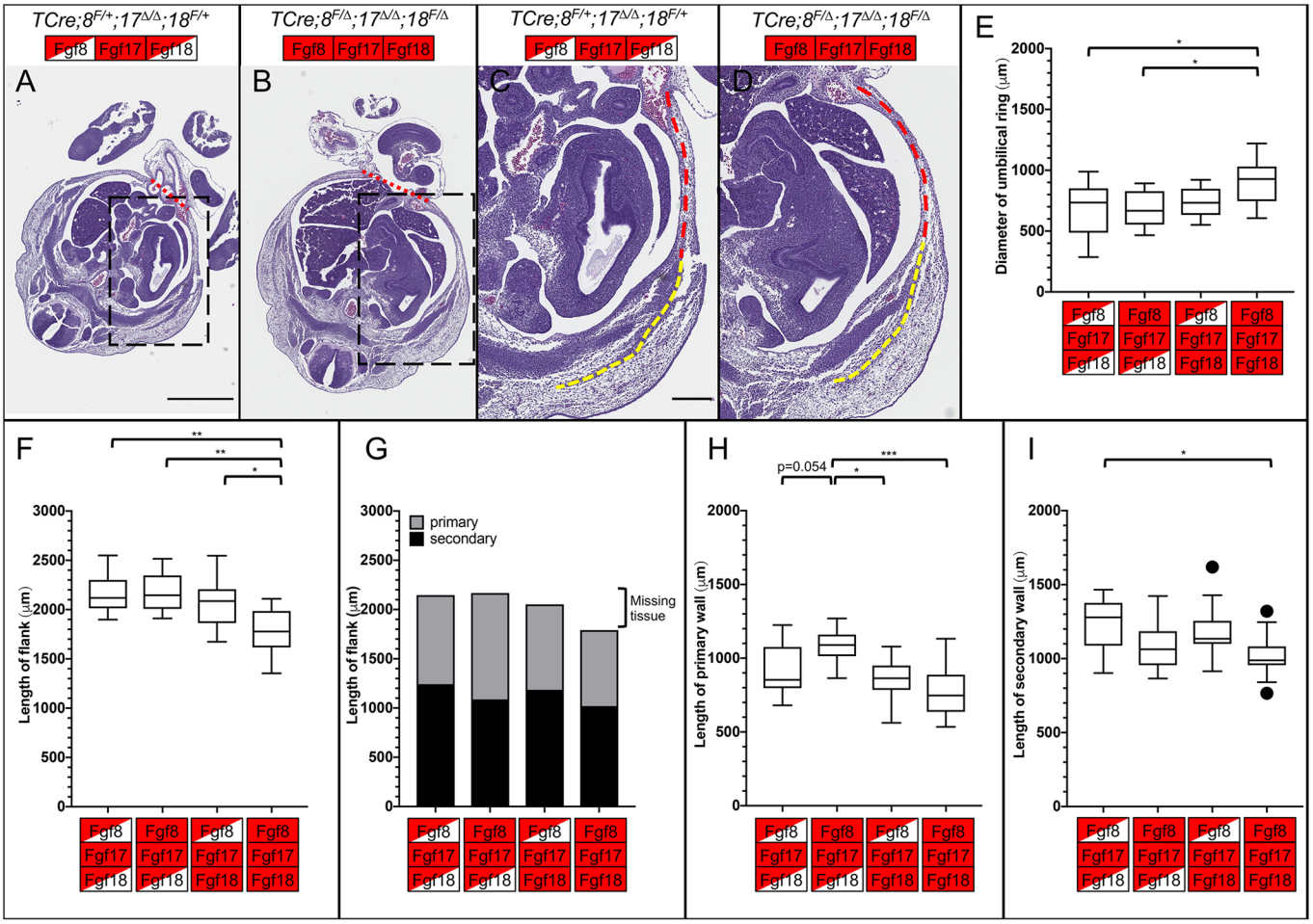

Fig. 5. Morphometric analysis of sections at E12.5 reveals changes in the primary and secondary VWs of *Fgf8* subfamily mutants preceding omphalocele. (A,B) Transverse section of E12.5 control (A) and triple mutant (B) embryo at the interlimb region of the axis. Note the absence of liver in the physiological hernia of triple mutants at this stage. Red dashed lines indicate diameter of the umbilical ring, as measured in E. (C,D) Enlargement of boxed regions of A (C) and B (D) showing the primary (red dashed line) and secondary (yellow dashed line) VWs. (E-I) Morphometric measurements of transverse sections of the indicated genotype. (E) Tukey box-pot of the diameter of the umbilical ring. (F) Tukey box-plot of the primary and secondary VW added together, to form the whole flank of the embryo. (G) Bar chart of the mean length of the primary and secondary VW. The reduction in the length of the flank in triple mutants is indicated (bracket). (H) Tukey box-plot of the primary VW. (I) Tukey box-plot of the secondary VW. Box plots show median values (middle bars) and first to third interquartile ranges (boxes); whiskers indicate 1.5× the interquartile ranges; outliers in box-plots are plotted individually. Control n=12; TCre;*Fgf8*$^{fl/\Delta}$,*17*$^{\Delta/\Delta}$,*18*$^{fl+}$ n=10; TCre;*Fgf8*$^{fl+}$,*17*$^{\Delta/\Delta}$,*18*$^{fl\Delta}$ n=11; triple mutant n=11. Significance was determined using a post-hoc Tukey-Kramer test. *P<0.05, **P<0.01, ***P<0.001. Boxes indicate genotype, see Fig. 2 for key. Scale bars: 1 mm (A); 250 µm (C).

significantly wider (Fig. 5E), showing that an increase in umbilical ring diameter precedes the herniation of the liver and suggesting that this could cause the omphalocele. An enlarged umbilical ring presumably comes at the expense of the embryonic flank and, indeed, when we measured the flank we found that in triple mutants the flank was significantly shorter (Fig. 5F,G). We examined the primary VW and secondary VW to see if one was more affected than the other. In triple mutants the length of the primary VW was no different from controls, though it did trend shorter (Fig. 5H). The thickness of the primary VW was also unaffected at this stage in triple mutants (Fig. S6F-J), though the primary VW is thinner in TCre;*Fgf8*$^{f/+}$;*Fgf17*$^{\Delta/\Delta}$;*Fgf18*$^{f/\Delta}$ embryos (Fig. S6I,J). The length of the secondary VW in triple mutants was significantly shorter than controls (Fig. 5I). TCre;*Fgf8*$^{f/\Delta}$;*Fgf17*$^{\Delta/\Delta}$;*Fgf18*$^{f/+}$ embryos and TCre;*Fgf8*$^{f/+}$;*Fgf17*$^{\Delta/\Delta}$;*Fgf18*$^{f/\Delta}$ embryos did not have a significantly shorter secondary VW, suggesting that one allele of *Fgf8* or *Fgf18* can rescue the length of the secondary VW at this embryonic stage. However, we did note that the TCre;*Fgf8*$^{f/\Delta}$;*Fgf17*$^{\Delta/\Delta}$;*Fgf18*$^{f/+}$ embryos trended towards a shorter secondary VW, suggesting that the secondary VW was beginning to be affected at E12.5 (Fig. 5I). The trend towards a longer primary VW in TCre;*Fgf8*$^{f/\Delta}$;*Fgf17*$^{\Delta/\Delta}$;*Fgf18*$^{f/+}$ embryos compared with controls (Fig. 5H) would explain why the total flank in TCre;*Fgf8*$^{f/\Delta}$;*Fgf17*$^{\Delta/\Delta}$;*Fgf18*$^{f/+}$ embryos is unchanged (Fig. 5F,G). We also examined proliferation and cell death at E12.5. Anti-pHH3 and activated c-caspase 3 co-immunostaining at E12.5 in the secondary VW of the embryo (Fig. S7A-D) did not reveal any changes between genotypes. This suggests that the reduction in secondary VW length is primarily due to a defect in migration from the somites, or because the somites were formed with less tissue before muscle formation.

In triple mutants the entire flank, which includes the primary and secondary VWs, was shorter than controls at E12.5 (Fig. 5F). We propose that in triple mutants these VW defects result in an enlarged umbilical ring and therefore a higher rate of omphalocele. At E13.5, all three mutant genotypes have a shorter flank than controls (Fig. 4E), and this reduction in length is largely the result of a shorter secondary VW (Fig. 4H). This reduction in length is most

Development (2020) 147, dev189506. doi:10.1242/dev.189506

pronounced in triple mutants. From these morphometric analyses we conclude that the VW defects we observe start earlier in triple mutants and are more severe than in TCre;*Fgf8*$^{f/\Delta}$;*Fgf17*$^{\Delta/\Delta}$;*Fgf18*$^{f/+}$ embryos and TCre;*Fgf8*$^{f/+}$;*Fgf17*$^{\Delta/\Delta}$;*Fgf18*$^{f/\Delta}$ embryos, strongly suggesting an additive genetic effect.

Fgf8 is required in the PSM and *Fgf18* is required in the somites to close the VW

Although we have been able to show that the *Fgf8* subfamily is needed for VW closure, we did not know when and where these genes are required. TCre recombination begins at E7.5 in the primitive streak and nascent PSM (Perantoni et al., 2005). Therefore, the structures that close the VW, the LPM-derived primary VW and the somite-derived abdominal muscles, will both contain deleted *Fgf* alleles. Although the expression of *Fgf17* is limited to the PSM, *Fgf8* and *Fgf18* are expressed in both the PSM and the somites, making it impossible to determine their spatial and temporal requirements using TCre. We decided to use two other Cre-expressing lines (see Table S1), the *Meox1*$^{tm1(cre)Jpa}$ (hereafter 'Meox1Cre') line, which recombines in the somites after segmentation (Jukkola et al., 2005), and the Tg(Cited1-cre/ERT2,-EGFP)1Mdca or Cited1CreER^{T2} (hereafter 'Cited1Cre') line, which recombines in the PSM and somites but not the primitive streak (Boyle et al., 2008; Garriock et al., 2015).

We used the *Gt(ROSA)26Sor*^{tm1Sor}/J (hereafter 'R26R') reporter line (Soriano, 1999) to examine the Meox1Cre recombination pattern. Recombination in the most posterior somites was incomplete; strong signal was only observed about four somites anterior to the PSM (Fig. S8A). We performed WISH against the floxed region of *Fgf8* (Fig. 6A,B) and *Fgf18* (Fig. 6C,D) to confirm that Cre recombination had occurred. In *Meox1Cre;Fgf8*$^{f/\Delta}$;*Fgf17*$^{\Delta/\Delta}$;*Fgf18*$^{f/\Delta}$ embryos we saw strong *Fgf8* expression in the PSM but no expression in the somites, as expected. We also observed an ectopic region of *Fgf8* expression in several caudal somites that we have determined is a consequence of losing a copy of *Meox1*, as Cre is inserted into the *Meox1* locus (Jukkola et al., 2005). In *Meox1Cre;*

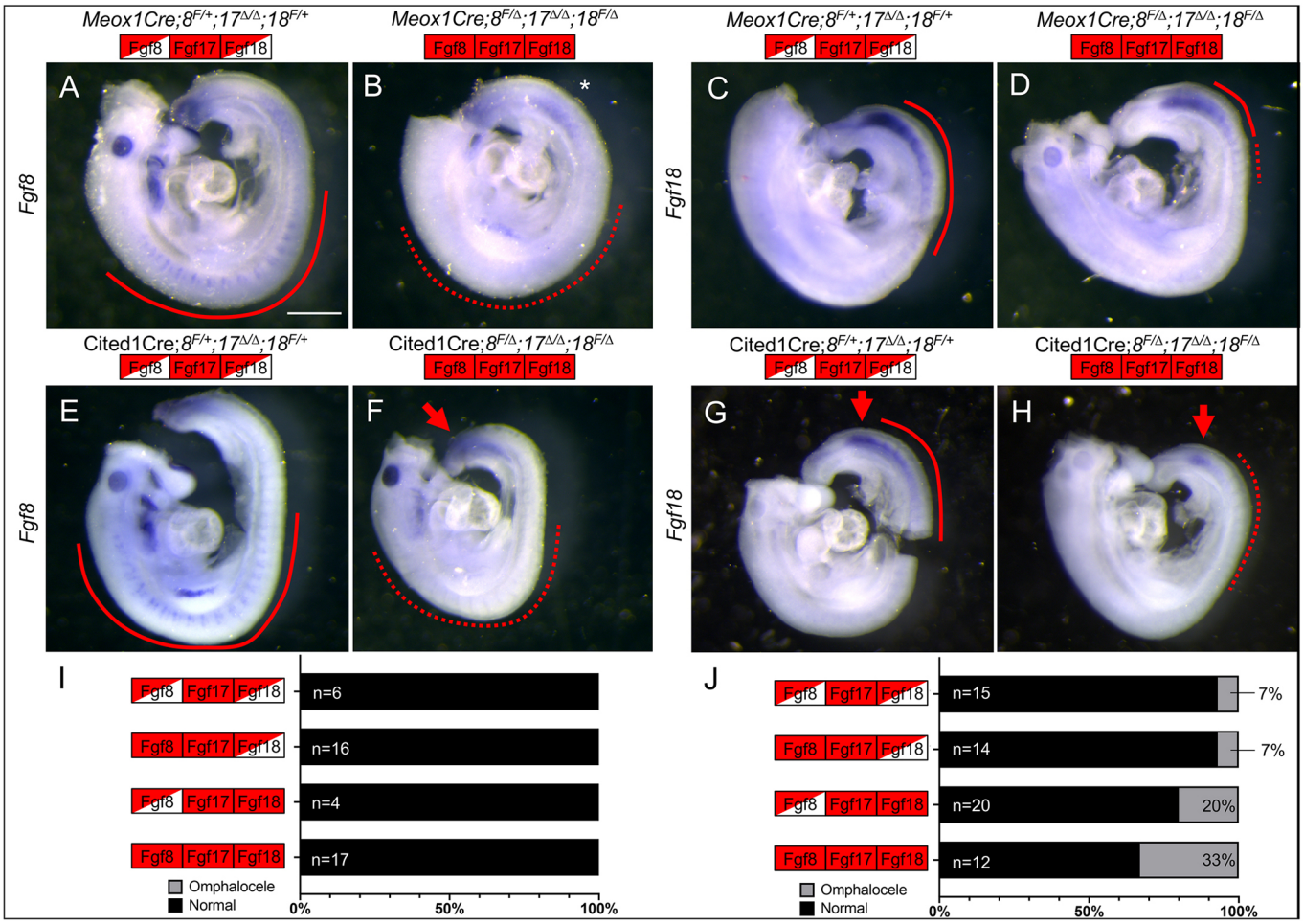

Fig. 6. Different tissue-specific Cre lines demonstrate requirement for *Fgf8* in PSM and *Fgf18* in somites. (A-D) WISH directed against floxed region of *Fgf8* (A,B) and *Fgf18* (C,D) in Meox1Cre;*Fgf8*$^{fl/+}$;*Fgf17*$^{\Delta/\Delta}$;*Fgf18*$^{fl/+}$ embryos (A,C) and Meox1Cre;*Fgf8*$^{fl/\Delta}$;*Fgf17*$^{\Delta/\Delta}$;*Fgf18*$^{fl/\Delta}$ embryos (B,D). Meox1Cre;*Fgf8*$^{fl/+}$;*Fgf17*$^{\Delta/\Delta}$;*Fgf18*$^{fl/+}$ embryos displayed normal expression of *Fgf8* (A) and *Fgf18* (C) in the somites (red line). Meox1Cre;*Fgf8*$^{fl/\Delta}$;*Fgf17*$^{\Delta/\Delta}$;*Fgf18*$^{fl/\Delta}$ embryos lost expression of *Fgf8* (B) in the somites (red dashed line), but *Fgf18* was mostly intact (D). Ectopic expression of *Fgf8* in Meox1Cre embryos (A,B), indicated by asterisk, compare with (E). (E-H) WISH directed against floxed region of *Fgf8* (E,F) and *Fgf18* (G,H) in Cited1Cre;*Fgf8*$^{fl/+}$;*Fgf17*$^{\Delta/\Delta}$;*Fgf18*$^{fl/+}$ embryos (E,G) and Cited1Cre;*Fgf8*$^{fl/\Delta}$;*Fgf17*$^{\Delta/\Delta}$;*Fgf18*$^{fl/\Delta}$ embryos (F,H). Cited1Cre;*Fgf8*$^{fl/\Delta}$;*Fgf17*$^{\Delta/\Delta}$;*Fgf18*$^{fl/\Delta}$ embryos lost expression of *Fgf8* (F) and *Fgf18* (H) in the somites (red dashed line). Note that expression of *Fgf8* in the PSM is unaffected in mutants (F, red arrow), and the expression of *Fgf18* is still present in the anterior PSM (H, red arrow). (I,J) Graphical representation of the incidence of omphalocele at E18.5 using Meox1Cre (I) and at E15.5 using Cited1Cre (J) showing the percentage of embryos with and without omphalocele. The total number of embryos is to the left of the bars and the percentage of embryos with omphalocele is on the right. Boxes indicate genotype, see Fig. 2 for key. Scale bar: 500 µm.

Development (2020) 147, dev189506. doi:10.1242/dev.189506

Fgf8$^{f/\Delta}$;*Fgf17*$^{\Delta/\Delta}$;*Fgf18*$^{f/\Delta}$ embryos we saw a restriction in the anterior extent of the somitic *Fgf18* expression and a slight decrease in transcript levels in the PSM and somites. *Meox1Cre;Fgf8*$^{f/\Delta}$;*Fgf17*$^{\Delta/\Delta}$;*Fgf18*$^{f/\Delta}$ embryos never presented with omphalocele at E18.5 (Fig. 6I, Fig. S8B). As recombination is complete in the dermomyotome by E9.5 (Jukkola et al., 2005), the downstream abdominal muscles will have been recombined, so there must be no later requirement in VW closure for *Fgf8* and *Fgf18* in this tissue lineage.

We next used the Cited1Cre line to recombine the *Fgf8* subfamily after tamoxifen induction (see Materials and Methods). We examined the recombination pattern in Cited1Cre;*R26R* embryos at E9.5 and saw complete recombination in the anterior PSM, the LPM and the somites throughout the axis, although the occipital somites remained unrecombined (Fig. S8C-G). We confirmed that robust recombination was observed caudal to the hindlimbs in E11.5 embryos (Fig. S8H), thus controlling gene expression in the somites that will give rise to the abdominal secondary VW. We checked that floxed alleles were recombined using WISH. *Fgf8* transcripts remained in the PSM, but not the somites, in *Cited1Cre;Fgf8*$^{f/+}$;*Fgf17*$^{\Delta/\Delta}$;*Fgf18*$^{f/\Delta}$ embryos (Fig. 6E,F). This is because the gradient of *Fgf8* mRNA in the PSM is a result of long-lived transcripts made in PSM progenitors in the caudal-most tailbud (Fig. S8I), outside the Cited1Cre expression domain (Dubrulle and Pourquié, 2004). *Fgf18* expression in the PSM was reduced and expression in the somites was abolished in Cited1Cre;*Fgf8*$^{f/+}$;*Fgf17*$^{\Delta/\Delta}$;*Fgf18*$^{f/\Delta}$ embryos (Fig. 6G,H).

We then scored omphalocele in embryos with Cited1Cre-mediated deletion of the *Fgf8* subfamily. Spontaneous abortions due to tamoxifen administration prevented recovery of E18.5 embryos often enough to impede our efforts. However, we reliably recovered E15.5 embryos at Mendelian ratios, which allowed analysis because the phenotype was evident by E13.5 (Fig. 3). In Cited1Cre;*Fgf8*$^{f/\Delta}$;*Fgf17*$^{\Delta/\Delta}$;*Fgf18*$^{f/+}$ embryos, the omphalocele incidence was very infrequent and equivalent to controls (one individual in each genotype) (Fig. 6J), suggesting that the loss of *Fgf8* expression in the somites (Fig. 6F) does not cause a VW closure defect and therefore the *Fgf8* requirement is in the PSM. In Cited1Cre;*Fgf8*$^{f/+}$;*Fgf17*$^{\Delta/\Delta}$;*Fgf18*$^{f/\Delta}$ embryos, the omphalocele frequency was similar to that observed in TCre;*Fgf8*$^{f/+}$;*Fgf17*$^{\Delta/\Delta}$;*Fgf18*$^{f/\Delta}$ embryos (Fig. 2G), suggesting the requirement for *Fgf18* in VW closure is in the somites. The lack of a phenotype in *Meox1Cre*;*Fgf8*$^{f/\Delta}$;*Fgf17*$^{\Delta/\Delta}$;*Fgf18*$^{f/\Delta}$ embryos is a result of two intact activities: *Fgf8* in the PSM and *Fgf18* in the somites (Fig. 6A-D). Cited1Cre;*Fgf8*$^{f/\Delta}$;*Fgf17*$^{\Delta/\Delta}$;*Fgf18*$^{f/\Delta}$ embryos displayed a 33% rate of omphalocele (Fig. 6J, Fig. S8J), which was significantly lower than the 71% observed in TCre;*Fgf8*$^{f/\Delta}$;*Fgf17*$^{\Delta/\Delta}$;*Fgf18*$^{f/\Delta}$ embryos (P=0.0139, two-tailed Fisher's exact test) because in the Cited1Cre;*Fgf8*$^{f/\Delta}$;*Fgf17*$^{\Delta/\Delta}$;*Fgf18*$^{f/\Delta}$ embryos the PSM domain of *Fgf8* remained intact (Fig. 6F).

From these results we conclude that the requirement for *Fgf8* expression is in the PSM; the hypothesis that *Fgf8* is required in the PSM is further supported by the fact that loss of *Fgf17* in TCre;*Fgf8*$^{f/\Delta}$ mutants promoted omphalocele (Fig. 2G), and *Fgf17* is expressed in the PSM but not the somites (Fig. 1). The requirement for the expression of *Fgf18* is in the anterior PSM and/or newly formed somites. The lack of a VW defect in *Meox1Cre;Fgf8*$^{f/\Delta}$;*Fgf17*$^{\Delta/\Delta}$;*Fgf18*$^{f/\Delta}$ embryos (Fig. 6I) suggests there is no requirement in the dermomyotome or later myotome or muscle lineages for *Fgf8* or *Fgf18*.

The *Fgf8* subfamily is required to maintain proper levels of progenitor tissue in the PSM and correctly sized somites

The results we have obtained thus far present something of a conundrum: how does the loss of *Fgf8* and *Fgf17* in the PSM cause omphalocele at E13.5 and later? As FGF signaling is known to be essential for both maintaining a pool of progenitor tissue within the PSM (Naiche et al., 2011) and for somitogenesis (Dubrulle et al., 2001), we looked for defects in these two processes in our TCre *Fgf8* subfamily conditional mutant mouse line. We chose the TCre line because triple mutants have the highest incidence of omphalocele, so we can analyze embryos that would likely have had omphalocele at a later gestational age. We performed WISH for both *Msgn1* and *Uncx4.1* (*Uncx*) at E9.5 (Fig. 7A,B) and at E10.5 (Fig. 7F,G), to label the progenitors of the paraxial mesoderm (Yoon et al., 2000) and the caudal half of each somite, respectively (Mansouri et al., 1997), in somite-stage matched E9.5 and E10.5 embryos.

Using *Uncx4.1* expression, at the 28-30 somite stage (E9.5) we could see a trend towards a smaller anterior-posterior (A-P) length in each somite throughout the length of triple mutants (Fig. 7C). We calculated the sum of the lengths of somites 12-27 (corresponding to the future thoracic and lumbar vertebrae) and found no differences between triple mutants and controls (Fig. 7D). We then examined the PSM, as a defect in the PSM could lead to somite defects. We observed that the *Msgn1* expression domain was shorter in triple mutants compared with controls (Fig. 7E). We also observed a shorter *Msgn1* expression domain in TCre;*Fgf8*$^{f/\Delta}$;*Fgf17*$^{\Delta/\Delta}$;*Fgf18*$^{f/+}$ but not TCre;*Fgf8*$^{f/+}$;*Fgf17*$^{\Delta/\Delta}$;*Fgf18*$^{f/\Delta}$ embryos compared with controls (Fig. 7E).

We then examined the expression of *Msgn1* and *Uncx4.1* approximately 24 h later (E10.5), at the 35-37 somite stage (Fig. 7F,G). We saw a far greater reduction in the A-P length of the somites of triple mutants compared with controls, with the length of multiple individual somites in the lower thoracic, lumbar and sacral region of the axis being smaller (Fig. 7H). There was a significant reduction in the sum of the A-P length of somites 14 through 35, which give rise to the vertebrae and muscles of the thorax and abdomen, in triple mutants compared with controls (Fig. 7I). As was the case at E9.5, there was a significant reduction in the length of the *Msgn1* domain in E10.5 triple mutants compared with controls (Fig. 7J). As was observed at E9.5, a reduction in the *Msgn1* domain was evident in TCre;*Fgf8*$^{f/\Delta}$;*Fgf17*$^{\Delta/\Delta}$;*Fgf18*$^{f/+}$ but not TCre;*Fgf8*$^{f/+}$;*Fgf17*$^{\Delta/\Delta}$;*Fgf18*$^{f/\Delta}$ embryos.

Together, the results of this paper show that *Fgf8*, but not *Fgf18*, is required for maintaining proper length of the PSM (as indicated by the *Msgn1* domain) and that in the absence of the *Fgf8* subfamily the size of the lumbar and sacral somites is reduced. The loss of *Fgf17*, which is expressed only in the PSM, likely contributes to this reduction of the PSM progenitor domain. Our genetic analysis shows that *Fgf8* and *Fgf17* are required in the PSM and that *Fgf18* is required in the somites (Fig. 8A). In controls, the migration of the secondary VW and size of the umbilical ring is normal (Fig. 8B), but in triple mutants the secondary VW is shorter and the umbilical ring is larger (Fig. 8C), which leads to omphalocele.

DISCUSSION

Inactivating multiple genes often reveals the complexity that underlies genetic interactions during embryogenesis. The 18 signaling members of the FGF ligand family frequently play numerous essential and redundant roles in development (reviewed by Ornitz and Itoh, 2015). Such interactions occur across subfamilies, such as the redundancy between *Fgf4* and *Fgf8* in maintenance of the undifferentiated PSM (Naiche et al., 2011) and in limb bud outgrowth (Boulet et al., 2004), *Fgf9* and *Fgf18* in skeletal development (Hung et al., 2016), or they occur within a

Development (2020) 147, dev189506. doi:10.1242/dev.189506

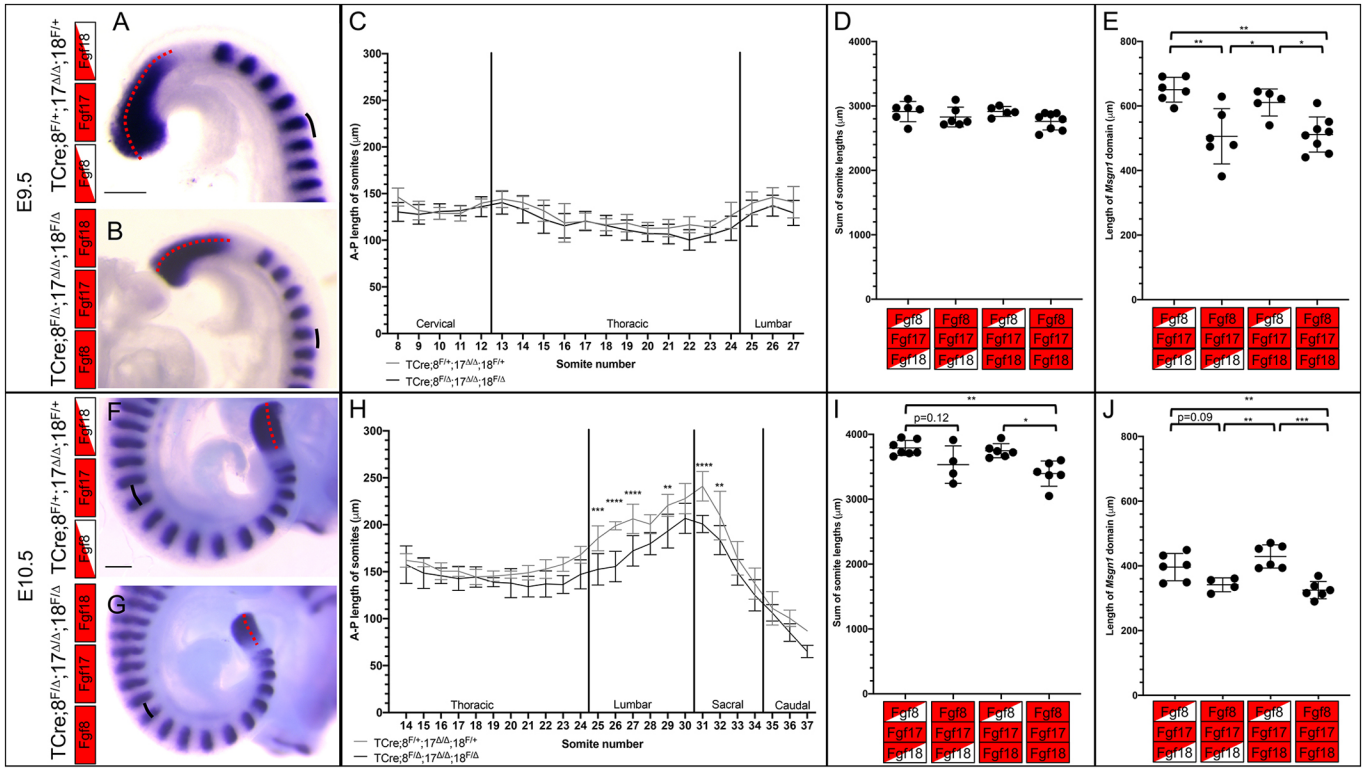

Fig. 7. Fgf8 is required to maintain the length of the *Msgn1* domain and the size of the somites. (A,B) Double WISH for *Msgn1* and *Uncx4.1* on E9.5 controls (A) and triple mutants (B). The length of the PSM (red dotted line) and the A-P length of the somites (black line indicates a representative example) were measured. (C) Graph of the A-P length of each somite for controls (gray line and bars, *n*=6) and triple mutants (black line and bars, *n*=8) at E9.5. Data are mean±s.d.; multiple *t*-test with Holm–Šidák correction applied. (D) Total A-P length of somites 12-24 at E9.5. (E) Length of the *Msgn1* domain. (F,G) Double WISH for *Msgn1* and *Uncx4.1* on E10.5 controls (F) and triple mutants (G). (H) Graph of the A-P length of each somite for controls (gray line and bars, *n*=7) and triple mutants (black line and bars, *n*=6) at E10.5. Data are mean±s.d., multiple *t*-test with Holm-Šidák correction applied. (I) The total A-P length of somites 14-35 at E10.5. (J) Length of *Msgn1* domain at E10.5. In panels D, E, I and J, data are individually plotted, mean and s.d. are shown, a post-hoc Tukey-Kramer test applied. ***P*<0.01, ****P*<0.001, *****P*<0.0001. Boxes indicate genotype, see Fig. 2 for key. Scale bars: 250 µm.

subfamily, such as between *Fgf8* and *Fgf17* in the hindbrain (Xu et al., 2000), *Fgf3* and *Fgf10* in otic placode and cardiovascular development (Urness et al., 2011; Wright and Mansour, 2003), *Fgf3* and *Fgf8* in otic placode development (Ladher et al., 2005), and *Fgf9* and *Fgf20* in cochlea, tooth and kidney development (Barak et al., 2012; Haara et al., 2012; Huh et al., 2015; Yang et al., 2019).

We present here the first evidence for genetic redundancy between all three members of the *Fgf8* subfamily. By inactivating

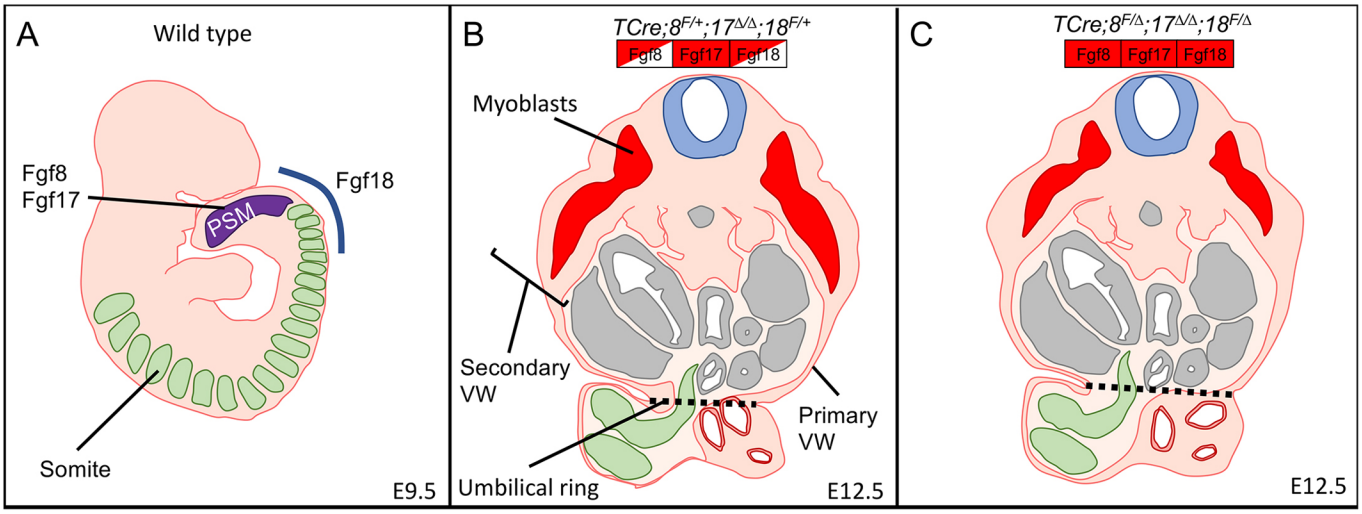

Fig. 8. Diagrams linking the spatial requirements of the *Fgf8* subfamily to VW morphogenesis. (A) Diagram of a wild-type E9.5 embryo showing *Fgf8* and *Fgf17* requirement in the PSM (purple) and *Fgf18* requirement in the anterior PSM (blue line). (B) Diagram of an E12.5 embryonic transverse section with the primary VW, secondary VW and umbilical ring (dotted line) indicated. (C) Triple mutant E12.5 embryonic transverse section showing smaller secondary VW and enlarged umbilical ring (dotted line).

Development (2020) 147, dev189506. doi:10.1242/dev.189506

these Fgf genes in different embryonic subsets using different tissue-specific Cre lines, we found that the activities of FGF8 and FGF17 are required in the PSM, and that FGF18 is required in the somites, in order to close the VW. By measuring somite and PSM progenitor domain length, we found that *Fgf8* and *Fgf17* appear to play a role in maintaining proper somite size. We propose that smaller somites cause a reduction in the amount of tissue in the secondary VW, and our morphometric analysis suggests that a loss of FGF18 activity can impair the secondary VW by delaying muscle migration. Defects in either somite size or muscle migration results in a low incidence of omphalocele, but when they occur simultaneously, the omphalocele incidence is greatly increased. This phenomenon, where defects in two separate processes result in a phenotype, is reminiscent of the *Fgf3;Fgf4* double mutant. In this mouse line a loss of *Fgf3* results in a reduction in levels of *Fgf8* (Anderson et al., 2016a) and as this is on an *Fgf4* mutant background, the FGF signal that maintains the PSM in an undifferentiated state is lost (Naiche et al., 2011). Consequently, the loss of tail vertebrae is more severe in the *Fgf3;Fgf4* double mutant than in *Fgf3* nulls alone (*Fgf4* mutants have a normal length tail) (Anderson et al., 2016b).

Furthermore, this study is the first to describe a role for FGF ligands in VW closure, and we demonstrate a gene dosage effect on the incidence of omphalocele. Omphalocele is also observed in *Fgfr1* heterozygotes, when *Fgfr2* is also conditionally inactivated at E8.5 throughout the embryo (Nichol et al., 2011). *Fgfr1* transcripts are detected in the PSM and both *Fgfr1* and *Fgfr2* genes are expressed in the somites and LPM at E8.5 and E9.5. (Orr-Urtreger et al., 1991; Wahl et al., 2007). Thus, the expression domains of these receptor genes are consistent with our model (Fig. 8). At E11.5-E13.5, these receptor genes are also expressed in the VW itself; *Fgfr1* in a broad domain and *Fgfr2* transcripts are detected in VW subsets (Nichol et al., 2011; Orr-Urtreger et al., 1991; Peters et al., 1992). These later expression domains of the *Fgfr* genes suggest that FGF signaling may act at multiple locations to close the VW, a complexity similar to the role of FGF signaling in limb development (Benazet and Zeller, 2009; Jin et al., 2018). If FGFs provide directional cues for secondary VW migration at these later stages, as they do during migration of tracheal cartilage (Elluru et al., 2009), our data suggest they may be encoded by Fgfs outside the *Fgf8* subfamily. This later FGF signaling step may be upstream of MEK1 and MEK2 function, which is required at these stages to close the VW (Boucherat et al., 2014). Future work will determine whether MEK1/2 kinases function downstream of the FGF8 subfamily in the PSM and somites.

In humans, omphalocele is reported in two case studies of Aperts syndrome (Ercoli et al., 2014; Herman and Siegel, 2010), which is caused by Fgfr2 mutations, but is otherwise known as a craniosynostosis pathology (Armand et al., 2019). Otherwise, there are no reports of mutations in Fgf ligands or receptors causing VW defects in humans, possibly because of genetic redundancy or embryonic lethality.

Kyphosis has been proposed as a causal factor in several mouse models of omphalocele (Boucherat et al., 2014; Kakizaki et al., 2015) with the rationale that a malpositioned spine could reduce the volume of the abdominal cavity and increase intra-abdominal pressure, forcing the viscera out through the umbilicus. We observed that triple mutants, compared with $TCre^{+};Fgf8^{f/+};Fgf17^{\Delta/\Delta};Fgf18^{f/\Delta}$ embryos, have both a greater rate of omphalocele and more severe kyphosis, suggesting spinal defects may exacerbate VW defects. However, it is not the case that kyphosis is the primary cause, because omphalocele occurs in $TCre^{+};Fgf8^{f/+};Fgf17^{\Delta/\Delta};Fgf18^{f/+}$ mutants, which lack kyphosis, demonstrating that VW defects occur with a normal spine. Furthermore, in human patients, once the omphalocele is repaired, the volume of the abdominal cavity and the posture of the spine both recover (Nagaya et al., 2000), suggesting omphalocele may cause spine defects. Therefore, any causality between kyphosis and omphalocele is unclear and warrants future study.

We see a measurable delay in mutant muscle migration at E12.5 and E13.5, and it has been proposed that muscle migration defects of the secondary VW are causative of omphalocele (Nichol et al., 2012). Defects in the primary VW have also been linked to VW closure defects (Brewer and Williams, 2004b), and it is known that the primary VW acts as a signaling center to promote secondary VW morphogenesis (Aldeiri et al., 2017; Brewer and Williams, 2004b; Nichol et al., 2011; Zhang et al., 2014). In triple mutants at E12.5 the whole flank is smaller and the umbilical ring is larger immediately before omphalocele. We speculate that as the embryo grows the viscera are forced through this enlarged opening.

Using multiple Cre lines, we determined the spatial and temporal requirements for the Fgf8 subfamily genes in VW closure. Consistent with the hypothesis that omphalocele is multifactorial in origin, we find that *Fgf8* and *Fgf17* are needed in the PSM whereas *Fgf18* is required in the somites. This requirement for *Fgf8* and *Fgf17* in the PSM is supported by the observation that in $TCre^{+};Fgf8^{f/\Delta};Fgf17^{\Delta/\Delta};Fgf18^{f/+}$ mutants, there is a reduction in the PSM *Msgn1* domain, which marks the progenitor pool of cells that form the mesoderm, including the LPM and the paraxial mesoderm. As a result, the somites are smaller and there is less material available to close the VW. This, combined with the secondary VW defects or the kyphosis caused by the loss of *Fgf18*, causes the high rates of omphalocele that we observe in triple mutants. In addition, we suggest that FGF signals do not provide directional cues per se for the secondary VW lineage, but are generally required for migration, as is the case for FGF signaling in limb and axis extension (Benazeraf et al., 2010; Gros et al., 2010; Lewandoski and Mackem, 2011). This idea is the focus of our future work. Our data highlight the complex and multifactorial origins of omphalocele and demonstrate that one simple overarching model for explaining its etiology is likely to be insufficient.

MATERIALS AND METHODS

Animal husbandry

Animals were maintained in accordance with the recommendations in the Guide for Care and Use of Laboratory Animals of the National Institutes of Health under a protocol approved by the Animal Care and Usage Committee of NCI at Frederick (NIH) (Animal Study Proposal: 17-069). Mice of both sexes were utilized, and all lines were maintained on an outbred background.

To conditionally delete *Fgf8* and *Fgf18* activity we used the previously described $Fgf8^{flox}$ line (Meyers et al., 1998) (hereafter $Fgf8^{f}$) and the $Fgf18^{flox}$ line (Hagan et al., 2019) (hereafter $Fgf18^{f}$). Null alleles of these genes as well as *Fgf17* were generated as previously described (Hagan et al., 2019; Meyers et al., 1998; Xu et al., 2000).

The TCre, Meox1Cre and Cited1Cre lines have all been described previously (Boyle et al., 2008; Jukkola et al., 2005; Perantoni et al., 2005). In order to generate experimental crosses, females homozygous for floxed alleles were mated to Cre recombinase-positive males. The same line of females was used for TCre, Meox1Cre and Cited1Cre experiments in which mutants for all three members of the *Fgf8* subfamily were generated. We used the $Gt(ROSA)26Sor^{tm1Sor}$/J (R26R) (Soriano, 1999) and $Gt(ROSA)26Sor^{tm4(ACTB\text{-}tdTomato,\text{-}EGFP)Luo}$/J (*mTmG*) lines (Muzumdar et al., 2007) to reveal Cre recombined tissues.

Tamoxifen administration

For embryonic experiments tamoxifen (40 mg/kg) and progesterone (40 mg/kg) were co-injected intraperitoneally into the same pregnant dams at 10:00 AM on

Development (2020) 147, dev189506. doi:10.1242/dev.189506

the morning of E7.5 and E8.5; embryos were collected at E15.5. This ensured that all mesoderm from the level of the heart until several somites caudal to the hindlimbs (i.e. past the sacral vertebrae) was recombined. To prepare, 100 mg of tamoxifen (Millipore-Sigma, T5648) was dissolved in 5 ml of corn oil (Millipore-Sigma, C8267) to which was added 5 ml of 50 mg/ml progesterone dissolved in sesame oil (Watson Pharma Inc., NDC 0591-3128-79). This was then sterilized through a 0.22 µm filter and stored at 4°C before use.

Wish

WISH was performed according to published protocols (Wilkinson and Nieto, 1993). In order to bring up regions of the embryo with relatively low levels of expression, development of the stain was prolonged. For the recombination probe experiment, controls and mutants were processed in the same vial and developed for the same length of time at 37°C. The *Fgf8* and especially the *Fgf18* recombination probes took considerable time to develop. We noticed that fainter domains of *Fgf18* were never labeled with the *Fgf18* recombination probe, presumably because the signal-to-noise ratio was too poor in these regions. Samples from E9.5 to E11.5 were cleared in 50% glycerol:PBS for several days before imaging. The *Fgf8*, *Fgf17* and *Fgf18* full-length probes have been previously reported (Maruoka et al., 1998), as has the *Fgf8* recombination probe (Perantoni et al., 2005). The PCR primers to generate the template for the *Fgf18* recombination probe (reverse primer also includes a T7 RNA polymerase promotor sequence) are: forwards, AGCCGAGGAGAATGTGGACT; reverse, TAATACGAC-TCACTATAGGGCCCAGGACTTGAATG-TGCTT.

Paraffin sections

For morphometric analyses of E12.5 and E13.5 embryos, samples were fixed overnight or longer in 10% neutral buffered formalin. They were taken through a graded series of ethanol dilutions before being infiltrated with xylene and then paraffin wax in a vacuum chamber. Then, 8 µm sections were taken and stained with Eosin and Hematoxylin (E12.5) or Masson's trichrome stain (E13.5). Stained slides were imaged and morphometric data obtained using Fiji image analysis software (Schindelin et al., 2012). For E18.5 embryos, samples were decapitated and the heart and lungs removed from the thoracic cavity before the whole sample was immersed in Bouin's solution for at least 7 days. Samples were then processed as for younger stages and stained with Masson's trichrome.

Morphometric analysis

A representative section for each stage-matched embryo was selected and all measurements were taken using that section. Sections were taken from the same axial level of the embryo and positionally matched using the stomach, kidneys, liver and gonads as anatomical markers.

Skeletal preparations

Alcian blue and Alizarin red co-staining was performed as previously described (Nagy et al., 2003).

Statistical analyses

When testing for significant differences in the rate of omphalocele between different genotypes or between different timepoints of the same genotype, a two-tailed Fisher's exact test was used. This test was also used when looking at the yolk sac defects at E10.5. When determining Mendelian ratios, a Chi-squared test was used. To perform multiple comparisons of the morphometric measurements of embryonic sections at E12.5 and E13.5, a post-hoc Tukey–Kramer test was used. This test was also used for the cell division and cell death analyses. In order to find whether there were differences between specific somites, a multiple *t*-test with a Holm-Šidák correction was used to account for type 1 errors (Holm, 1979). When investigating the total A-P length of the somites, and for investigating the length of the *Msgn1* domain, a post-hoc Tukey–Kramer test was used.

Antibody staining

Samples were fixed overnight at 4°C in 4% paraformaldehyde, then dehydrated and infiltrated with paraffin by hand. After sectioning, samples were dewaxed, subjected to antigen retrieval and stained according to Anderson et al. (2016a) with the following modifications: Citrisolv (Thermo Fisher Scientific) was used for dewaxing, sodium citrate buffer containing 0.05% Tween 20 (Sigma-Aldrich) and 10% normal goat serum (Sigma-Aldrich) in PTX was used for dilution of blocking and antibodies. Primary antibodies used were anti-phospho histone H3 (Cell Signaling Technologies, 9706L, 1:500) and anti-cleaved caspase 3 (Cell Signaling Technologies, 9661L, 1:250). Secondary antibodies used were goat anti-mouse Alexa Fluor 594 (Thermo Fisher Scientific, A-32740) and goat anti-rabbit Alexa Fluor 647 (Thermo Fisher Scientific, A-21244). Immunocomplexes were detected using a Zeiss LSM710 confocal microscope using a 20× objective to generate tiled *z*-stacks. Nuclei were counted using Imaris image analysis software (Oxford instruments). pHH3- and cleaved caspase 3-positive cells were counted manually using maximum projections of *z*-stacks. Three sections per embryo were analyzed to generate results in triplicate.

HCR

HCR was performed as previously described (Choi et al., 2018) with modifications as described in Anderson et al. (2020 preprint). Probes against *Fgf8*, *Fgf17* and *Fgf18* were designed by Molecular Instruments and were hybridized with hairpins conjugated to Alexa Fluor 647, Alexa Fluor 546 and Alexa Fluor 488 (Molecular Instruments), respectively. After hybridization, samples were embedded in ultra low melt agarose on a glass bottomed dish and cleared in Ce3D as previously described (Anderson et al., 2020 preprint; Li et al., 2017). After clearing, samples were imaged on a Nikon A1 confocal microscope and captured *z*-stacks were processed in FiJi (Schindelin et al., 2012).

β-galactosidase staining

Pregnant dams were euthanized and embryos were dissected out as previously described. Embryos were then fixed for 40 min at room temperature in fixation buffer (1% formaldehyde, 0.2% glutaraldehyde, 2 mM $MgCl_2$, 5 mM EGTA and 0.02% NP-40 in PBS). Embryos were then washed 3×10 min in 0.02% NP-40 in PBS solution. Embryos were then incubated at 37°C overnight in stain solution (5 mM potassium ferricyanide, 5 mM potassium ferrocyanide, 2 mM $MgCl_2$, 0.01% sodium deoxycholate, 0.02% NP-40, 1 mg/ml X-gal in PBS), After staining was complete, embryos were washed in PBS and then post fixed in 4% paraformaldehyde at 4°C overnight. For whole-mount imaging embryos were then washed in PBS, cleared in 50% glycerol and imaged. Embryos for sectioning were put through a dehydration ethanol series, embedded in paraffin and 8 µm sections were taken on a microtome (Lecia Reichert Jung BioCut 2030). Slides were then dewaxed, stained with Nuclear Fast Red and then coverslipped and imaged.

Genotyping primers

Fgf18 flox: forwards, ATTCAGGAGCAGCTCAGTCC; reverse, TGTC-ATGACCTGATGGCAAC. Fgf18 delta: forwards, CCTGGGGCTGTGG-GAAAATA; reverse, GCCTGGGGTTGATGTGTACT. TCre: forwards, GCTGTTGGGTAGGGAGTCAA; reverse, ATGTTTAGCTGGCCCA-AATG.

Acknowledgements

We are grateful for technical assistance from M. Brown, C. Elder and E. Truffer. We also thank J. Matta and the Histopathology Lab (NCI at Frederick) for generating tissue sections and the NCI Optical Microscopy and Image Analysis Lab for confocal imagery. We thank members of the Lewandoski lab and the Cancer and Developmental Biology Lab-NCI for helpful discussions.

Competing interests

The authors declare no competing or financial interests.

Author contributions

Conceptualization: M.L., M.B.; Methodology: M.L., M.B., M.J.A.; Validation: M.B.; Formal analysis: M.B., M.J.A., D.M.O.; Investigation: M.L., M.B., M.J.A.; Resources: M.L., D.M.O.; Writing - original draft: M.B.; Writing - review & editing: M.L., M.B., M.J.A., D.M.O.; Visualization: M.B.; Supervision: M.L.; Project administration: M.L.; Funding acquisition: M.L.

Funding

This work was supported by the Center for Cancer Research of the Intramural Research Program of the National Institutes of Health through the National Cancer

Institute; the National Heart, Lung, and Blood Institute grant HL154747 to D.M.O.; and Washington University Musculoskeletal Research Center grant NIH P30 AR074992. Deposited in PMC for immediate release.

Supplementary information

Supplementary information available online at
https://dev.biologists.org/lookup/doi/10.1242/dev.189506.supplemental

Peer review history

The peer review history is available online at
https://dev.biologists.org/lookup/doi/10.1242/dev.189506.reviewer-comments.pdf

References

Aldeiri, B., Roostalu, U., Albertini, A., Wong, J., Morabito, A. and Cossu, G. (2017). Transgelin-expressing myofibroblasts orchestrate ventral midline closure through TGFbeta signalling. *Development* **144**, 3336-3348. doi:10.1242/dev.152843

Anderson, M. J., Schimmang, T. and Lewandoski, M. (2016a). An FGF3-BMP signaling axis regulates caudal neural tube closure, neural crest specification and anterior-posterior axis extension. *PLoS Genet.* **12**, e1006018. doi:10.1371/journal.pgen.1006018

Anderson, M. J., Southon, E., Tessarollo, L. and Lewandoski, M. (2016b). Fgf3-Fgf4-cis: a new mouse line for studying Fgf functions during mouse development. *Genesis* **54**, 91-98. doi:10.1002/dvg.22913

Anderson, M. J., Magidson, V., Kageyama, R. and Lewandoski, M. (2020). Fgf4 is critical for maintaining Hes7 levels and Notch oscillations in the somite segmentation clock. *BioRxiv*. doi:10.1101/2020.02.12.945931

Armand, T., Schaefer, E., Di Rocco, F., Edery, P., Collet, C. and Rossi, M. (2019). Genetic bases of craniosynostoses: an update. *Neurochirurgie* **65**, 196-201. doi:10.1016/j.neuchi.2019.10.003

Barak, H., Huh, S.-H., Chen, S., Jeanpierre, C., Martinovic, J., Parisot, M., Bole-Feysot, C., Nitschké, P., Salomon, R., Antignac, C. et al. (2012). FGF9 and FGF20 maintain the stemness of nephron progenitors in mice and man. *Dev. Cell* **22**, 1191-1207. doi:10.1016/j.devcel.2012.04.018

Bénazéraf, B., Francois, P., Baker, R. E., Denans, N., Little, C. D. and Pourquié, O. (2010). A random cell motility gradient downstream of FGF controls elongation of an amniote embryo. *Nature* **466**, 248-252. doi:10.1038/nature09151

Benazet, J.-D. and Zeller, R. (2009). Vertebrate limb development: moving from classical morphogen gradients to an integrated 4-dimensional patterning system. *Cold Spring Harb. Perspect Biol.* **1**, a001339. doi:10.1101/cshperspect.a001339

Boucherat, O., Nadeau, V., Berube-Simard, F.-A., Charron, J. and Jeannotte, L. (2014). Crucial requirement of ERK/MAPK signaling in respiratory tract development. *Development* **141**, 3197-3211. doi:10.1242/dev.110254

Boulet, A. M., Moon, A. M., Arenkiel, B. R. and Capecchi, M. R. (2004). The roles of Fgf4 and Fgf8 in limb bud initiation and outgrowth. *Dev. Biol.* **273**, 361-372. doi:10.1016/j.ydbio.2004.06.012

Boyle, S., Misfeldt, A., Chandler, K. J., Deal, K. K., Southard-Smith, E. M., Mortlock, D. P., Baldwin, H. S. and de Caestecker, M. (2008). Fate mapping using Cited1-CreERT2 mice demonstrates that the cap mesenchyme contains self-renewing progenitor cells and gives rise exclusively to nephronic epithelia. *Dev. Biol.* **313**, 234-245. doi:10.1016/j.ydbio.2007.10.014

Brewer, S. and Williams, T. (2004a). Finally, a sense of closure? Animal models of human ventral body wall defects. *BioEssays* **26**, 1307-1321. doi:10.1002/bies.20137

Brewer, S. and Williams, T. (2004b). Loss of AP-2α impacts multiple aspects of ventral body wall development and closure. *Dev. Biol.* **267**, 399-417. doi:10.1016/j.ydbio.2003.11.021

Carnaghan, H., Roberts, T., Savery, D., Norris, F. C., McCann, C. J., Copp, A. J., Scambler, P. J., Lythgoe, M. F., Greene, N. D., Decoppi, P. et al. (2013). Novel exomphalos genetic mouse model: the importance of accurate phenotypic classification. *J. Pediatr. Surg.* **48**, 2036-2042. doi:10.1016/j.jpedsurg.2013.04.010

Choi, H. M. T., Schwarzkopf, M., Fornace, M. E., Acharya, A., Artavanis, G., Stegmaier, J., Cunha, A. and Pierce, N. A. (2018). Third-generation in situ hybridization chain reaction: multiplexed, quantitative, sensitive, versatile, robust. *Development* **145**, dev165753. doi:10.1101/285213

Cholfin, J. A. and Rubenstein, J. L. R. (2007). Patterning of frontal cortex subdivisions by Fgf17. *Proc. Natl. Acad. Sci. USA* **104**, 7652-7657. doi:10.1073/pnas.0702225104

Corey, K. M., Hornik, C. P., Laughon, M. M., McHutchison, K., Clark, R. H. and Smith, P. B. (2014). Frequency of anomalies and hospital outcomes in infants with gastroschisis and omphalocele. *Early Hum. Dev.* **90**, 421-424. doi:10.1016/j.earlhumdev.2014.05.006

Crossley, P. H. and Martin, G. R. (1995). The mouse Fgf8 gene encodes a family of polypeptides and is expressed in regions that direct outgrowth and patterning in the developing embryo. *Development* **121**, 439-451.

Crossley, P. H., Minowada, G., MacArthur, C. A. and Martin, G. R. (1996). Roles for FGF8 in the induction, initiation, and maintenance of chick limb development. *Cell* **84**, 127-136. doi:10.1016/S0092-8674(00)80999-X

Dubrulle, J. and Pourquié, O. (2004). fgf8 mRNA decay establishes a gradient that couples axial elongation to patterning in the vertebrate embryo. *Nature* **427**, 419-422. doi:10.1038/nature02216

Dubrulle, J., McGrew, M. J. and Pourquie, O. (2001). FGF signaling controls somite boundary position and regulates segmentation clock control of spatiotemporal Hox gene activation. *Cell* **106**, 219-232. doi:10.1016/S0092-8674(01)00437-8

Elluru, R. G., Thompson, F. and Reece, A. (2009). Fibroblast growth factor 18 gives growth and directional cues to airway cartilage. *Laryngoscope* **119**, 1153-1165. doi:10.1002/lary.20157

Ercoli, G., Bidondo, M. P., Senra, B. C. and Groisman, B. (2014). Apert syndrome with omphalocele: a case report. *Birth Defects Res. A Clin. Mol. Teratol* **100**, 726-729. doi:10.1002/bdra.23270

Garriock, R. J., Chalamalasetty, R. B., Kennedy, M. W., Canizales, L. C., Lewandoski, M. and Yamaguchi, T. P. (2015). Lineage tracing of neuromesodermal progenitors reveals novel Wnt-dependent roles in trunk progenitor cell maintenance and differentiation. *Development* **142**, 1628-1638. doi:10.1242/dev.111922

Grifone, R., Demignon, J., Houbron, C., Souil, E., Niro, C., Seller, M. J., Hamard, G. and Maire, P. (2005). Six1 and Six4 homeoproteins are required for Pax3 and Mrf expression during myogenesis in the mouse embryo. *Development* **132**, 2235-2249. doi:10.1242/dev.01773

Gros, J., Hu, J. K.-H., Vinegoni, C., Feruglio, P. F., Weissleder, R. and Tabin, C. J. (2010). WNT5A/JNK and FGF/MAPK pathways regulate the cellular events shaping the vertebrate limb bud. *Curr. Biol.* **20**, 1993-2002. doi:10.1016/j.cub.2010.09.063

Haara, O., Harjunmaa, E., Lindfors, P. H., Huh, S.-H., Fliniaux, I., Aberg, T., Jernvall, J., Ornitz, D. M., Mikkola, M. L. and Thesleff, I. (2012). Ectodysplasin regulates activator-inhibitor balance in murine tooth development through Fgf20 signaling. *Development* **139**, 3189-3199. doi:10.1242/dev.079558

Hagan, A. S., Boylan, M., Smith, C., Perez-Santamarina, E., Kowalska, K., Hung, I. H., Lewis, R. M., Hajihosseini, M. K., Lewandoski, M. and Ornitz, D. M. (2019). Generation and validation of novel conditional flox and inducible Cre alleles targeting fibroblast growth factor 18 (Fgf18). *Dev. Dyn.* **248**, 882-893. doi:10.1002/dvdy.85

Herman, T. E. and Siegel, M. J. (2010). Apert syndrome with omphalocele. *J. Perinatol.* **30**, 695-697. doi:10.1038/jp.2010.72

Holm, S. (1979). A simple sequentially rejective multiple test procedure. *Scand. J. Stat.* **6**, 65-70.

Huh, S. H., Warchol, M. E. and Ornitz, D. M. (2015). Cochlear progenitor number is controlled through mesenchymal FGF receptor signaling. *Elife* **4**, e05921. doi:10.7554/eLife.05921.016

Hung, I. H., Schoenwolf, G. C., Lewandoski, M. and Ornitz, D. M. (2016). A combined series of Fgf9 and Fgf18 mutant alleles identifies unique and redundant roles in skeletal development. *Dev. Biol.* **411**, 72-84. doi:10.1016/j.ydbio.2016.01.008

Jin, L., Wu, J., Bellusci, S. and Zhang, J.-S. (2018). Fibroblast growth factor 10 and vertebrate limb development. *Front. Genet.* **9**, 705. doi:10.3389/fgene.2018.00705

Jukkola, T., Trokovic, R., Maj, P., Lamberg, A., Mankoo, B., Pachnis, V., Savilahti, H. and Partanen, J. (2005). Meox1Cre: a mouse line expressing Cre recombinase in somitic mesoderm. *Genesis* **43**, 148-153. doi:10.1002/gene.20163

Kakizaki, T., Oriuchi, N. and Yanagawa, Y. (2015). GAD65/GAD67 double knockout mice exhibit intermediate severity in both cleft palate and omphalocele compared with GAD67 knockout and VGAT knockout mice. *Neuroscience* **288**, 86-93. doi:10.1016/j.neuroscience.2014.12.030

Kitagaki, J., Ueda, Y., Chi, X., Sharma, N., Elder, C. M., Truffer, E., Costantini, F., Lewandoski, M. and Perantoni, A. O. (2011). FGF8 is essential for formation of the ductal system in the male reproductive tract. *Development* **138**, 5369-5378. doi:10.1242/dev.051888

Ladher, R. K., Wright, T. J., Moon, A. M., Mansour, S. L. and Schoenwolf, G. C. (2005). FGF8 initiates inner ear induction in chick and mouse. *Genes Dev.* **19**, 603-613. doi:10.1101/gad.1273605

Lewandoski, M. and Mackem, S. (2011). Developmental biology: extending the limb and body with vectors and scalars. *Curr. Biol.* **21**, R34-R36. doi:10.1016/j.cub.2010.11.023

Lewandoski, M., Sun, X. and Martin, G. R. (2000). Fgf8 signalling from the AER is essential for normal limb development. *Nat. Genet.* **26**, 460-463. doi:10.1038/82609

Li, W., Germain, R. N. and Gerner, M. Y. (2017). Multiplex, quantitative cellular analysis in large tissue volumes with clearing-enhanced 3D microscopy (Ce3D). *Proc. Natl. Acad. Sci. USA* **114**, E7321-E7330. doi:10.1073/pnas.1708981114

Liu, Z., Xu, J., Colvin, J. S. and Ornitz, D. M. (2002). Coordination of chondrogenesis and osteogenesis by fibroblast growth factor 18. *Genes Dev.* **16**, 859-869. doi:10.1101/gad.965602

Liu, Z., Lavine, K. J., Hung, I. H. and Ornitz, D. M. (2007). FGF18 is required for early chondrocyte proliferation, hypertrophy and vascular invasion of the growth plate. *Dev. Biol.* **302**, 80-91. doi:10.1016/j.ydbio.2006.08.071

Mansouri, A., Yokota, Y., Wehr, R., Copeland, N. G., Jenkins, N. A. and Gruss, P. (1997). Paired-related murine homeobox gene expressed in the developing sclerotome, kidney, and nervous system. *Dev. Dyn.* **210**, 53-65. doi:10.1002/(SICI)1097-0177(199709)210:1<53::AID-AJA6>3.0.CO;2-0

Marshall, J., Salemi, J. L., Tanner, J. P., Ramakrishnan, R., Feldkamp, M. L., Marengo, L. K., Meyer, R. E., Druschel, C. M., Rickard, R., Kirby, R. S. et al. (2015). Prevalence, correlates, and outcomes of omphalocele in the United States, 1995-2005. *Obstet. Gynecol.* **126**, 284-293. doi:10.1097/AOG.0000000000000920

Maruoka, Y., Ohbayashi, N., Hoshikawa, M., Itoh, N., Hogan, B. L. M. and Furuta, Y. (1998). Comparison of the expression of three highly related genes, Fgf8, Fgf17 and Fgf18, in the mouse embryo. *Mech. Dev.* **74**, 175-177. doi:10.1016/S0925-4773(98)00061-6

Matsumaru, D., Haraguchi, R., Moon, A. M., Satoh, Y., Nakagata, N., Yamamura, K., Takahashi, N., Kitazawa, S. and Yamada, G. (2014). Genetic analysis of the role of Alx4 in the coordination of lower body and external genitalia formation. *Eur. J. Hum. Genet.* **22**, 350-357. doi:10.1038/ejhg.2013.160

Meyers, E. N., Lewandoski, M. and Martin, G. R. (1998). An Fgf8 mutant allelic series generated by Cre- and Flp-mediated recombination. *Nat. Genet.* **18**, 136-141. doi:10.1038/ng0298-136

Murdoch, J. N., Damrau, C., Paudyal, A., Bogani, D., Wells, S., Greene, N. D. E., Stanier, P. and Copp, A. J. (2014). Genetic interactions between planar cell polarity genes cause diverse neural tube defects in mice. *Dis. Model. Mech.* **7**, 1153-1163. doi:10.1242/dmm.016758

Muzumdar, M. D., Tasic, B., Miyamichi, K., Li, L. and Luo, L. (2007). A global double-fluorescent Cre reporter mouse. *Genesis* **45**, 593-605. doi:10.1002/dvg.20335

Nagaya, M., Kato, J., Niimi, N. and Tanaka, S. (2000). Lordosis of lumbar vertebrae in omphalocele: an important factor in regulating abdominal cavity capacity. *J. Pediatr. Surg.* **35**, 1782-1785. doi:10.1053/jpsu.2000.19252

Nagy, A., Gertsenstein, M., Vintersten, K. and Behringer, R. (2003). *Manipulating the Mouse Embryo: A Laboratory Manual*, 3nd edn. University of Michigan: Cold Spring Harbor Laboratory Press.

Naiche, L. A., Holder, N. and Lewandoski, M. (2011). FGF4 and FGF8 comprise the wavefront activity that controls somitogenesis. *Proc. Natl. Acad. Sci. USA* **108**, 4018-4023. doi:10.1073/pnas.1007417108

Nichol, P. F., Corliss, R. F., Tyrrell, J. D., Graham, B., Reeder, A. and Saijoh, Y. (2011). Conditional mutation of fibroblast growth factor receptors 1 and 2 results in an omphalocele in mice associated with disruptions in ventral body wall muscle formation. *J. Pediatr. Surg.* **46**, 90-96. doi:10.1016/j.jpedsurg.2010.09.066

Nichol, P. F., Corliss, R. F., Yamada, S., Shiota, K. and Saijoh, Y. (2012). Muscle patterning in mouse and human abdominal wall development and omphalocele specimens of humans. *Anat. Rec. (Hoboken)* **295**, 2129-2140. doi:10.1002/ar.22556

Ohbayashi, N., Shibayama, M., Kurotaki, Y., Imanishi, M., Fujimori, T., Itoh, N. and Takada, S. (2002). FGF18 is required for normal cell proliferation and differentiation during osteogenesis and chondrogenesis. *Genes Dev.* **16**, 870-879. doi:10.1101/gad.965702

Ornitz, D. M. and Itoh, N. (2015). The fibroblast growth factor signaling pathway. *Wiley Interdiscip Rev. Dev. Biol.* **4**, 215-266. doi:10.1002/wdev.176

Orr-Urtreger, A., Givol, D., Yayon, A., Yarden, Y. and Lonai, P. (1991). Developmental expression of two murine fibroblast growth factor receptors, flg and bek. *Development* **113**, 1419-1434.

Perantoni, A. O., Timofeeva, O., Naillat, F., Richman, C., Pajni-Underwood, S., Wilson, C., Vainio, S., Dove, L. F. and Lewandoski, M. (2005). Inactivation of FGF8 in early mesoderm reveals an essential role in kidney development. *Development* **132**, 3859-3871. doi:10.1242/dev.01945

Peters, K. G., Werner, S., Chen, G. and Williams, L. T. (1992). Two FGF receptor genes are differentially expressed in epithelial and mesenchymal tissues during limb formation and organogenesis in the mouse. *Development* **114**, 233-243.

Rudnicki, M. A., Schnegelsberg, P. N., Stead, R. H., Braun, T., Arnold, H. H. and Jaenisch, R. (1993). MyoD or Myf-5 is required for the formation of skeletal muscle. *Cell* **75**, 1351-1359. doi:10.1016/0092-8674(93)90621-V

Scearce-Levie, K., Roberson, E. D., Gerstein, H., Cholfin, J. A., Mandiyan, V. S., Shah, N. M., Rubenstein, J. L. and Mucke, L. (2008). Abnormal social behaviors in mice lacking Fgf17. *Genes Brain Behav.* **7**, 344-354. doi:10.1111/j.1601-183X.2007.00357.x

Schindelin, J., Arganda-Carreras, I., Frise, E., Kaynig, V., Longair, M., Pietzsch, T., Preibisch, S., Rueden, C., Saalfeld, S., Schmid, B. et al. (2012). Fiji: an open-source platform for biological-image analysis. *Nat. Methods* **9**, 676-682. doi:10.1038/nmeth.2019

Soriano, P. (1999). Generalized lacZ expression with the ROSA26 Cre reporter strain. *Nat. Genet.* **21**, 70-71. doi:10.1038/5007

Stoll, C., Alembik, Y., Dott, B. and Roth, M.-P. (2008). Omphalocele and gastroschisis and associated malformations. *Am. J. Med. Genet. A* **146A**, 1280-1285. doi:10.1002/ajmg.a.32297

Stolte, D., Huang, R. and Christ, B. (2002). Spatial and temporal pattern of Fgf-8 expression during chicken development. *Anat. Embryol. (Berl)* **205**, 1-6. doi:10.1007/s00429-002-0227-z

Sun, X., Meyers, E. N., Lewandoski, M. and Martin, G. R. (1999). Targeted disruption of Fgf8 causes failure of cell migration in the gastrulating mouse embryo. *Genes Dev.* **13**, 1834-1846. doi:10.1101/gad.13.14.1834

Tremblay, P., Dietrich, S., Mericskay, M., Schubert, F. R., Li, Z. and Paulin, D. (1998). A crucial role for Pax3 in the development of the hypaxial musculature and the long-range migration of muscle precursors. *Dev. Biol.* **203**, 49-61. doi:10.1006/dbio.1998.9041

Urness, L. D., Bleyl, S. B., Wright, T. J., Moon, A. M. and Mansour, S. L. (2011). Redundant and dosage sensitive requirements for Fgf3 and Fgf10 in cardiovascular development. *Dev. Biol.* **356**, 383-397. doi:10.1016/j.ydbio.2011.05.671

Wahl, M. B., Deng, C., Lewandoski, M. and Pourquie, O. (2007). FGF signaling acts upstream of the NOTCH and WNT signaling pathways to control segmentation clock oscillations in mouse somitogenesis. *Development* **134**, 4033-4041. doi:10.1242/dev.009167

Wilkinson, D. G. and Nieto, M. A. (1993). Detection of messenger RNA by in situ hybridization to tissue sections and whole mounts. *Methods Enzymol.* **225**, 361-373. doi:10.1016/0076-6879(93)25025-W

Williams, T. (2008). Animal models of ventral body wall closure defects: a personal perspective on gastroschisis. *Am. J. Med. Genet. C Semin. Med. Genet.* **148C**, 186-191. doi:10.1002/ajmg.c.30179

Wright, T. J. and Mansour, S. L. (2003). Fgf3 and Fgf10 are required for mouse otic placode induction. *Development* **130**, 3379-3390. doi:10.1242/dev.00555

Xu, J., Lawshé, A., MacArthur, C. A. and Ornitz, D. M. (1999). Genomic structure, mapping, activity and expression of fibroblast growth factor 17. *Mech. Dev.* **83**, 165-178. doi:10.1016/S0925-4773(99)00034-9

Xu, J., Liu, Z. and Ornitz, D. M. (2000). Temporal and spatial gradients of Fgf8 and Fgf17 regulate proliferation and differentiation of midline cerebellar structures. *Development* **127**, 1833-1843.

Yang, L. M., Cheah, K. S. E., Huh, S.-H. and Ornitz, D. M. (2019). Sox2 and FGF20 interact to regulate organ of Corti hair cell and supporting cell development in a spatially-graded manner. *PLoS Genet.* **15**, e1008254. doi:10.1371/journal.pgen.1008254

Yoon, J. K., Moon, R. T. and Wold, B. (2000). The bHLH class protein pMesogenin1 can specify paraxial mesoderm phenotypes. *Dev. Biol.* **222**, 376-391. doi:10.1006/dbio.2000.9717

Zhang, L., Li, H., Yu, J., Cao, J., Chen, H., Zhao, H., Zhao, J., Yao, Y., Cheng, H., Wang, L. et al. (2014). Ectodermal Wnt signaling regulates abdominal myogenesis during ventral body wall development. *Dev. Biol.* **387**, 64-72. doi:10.1016/j.ydbio.2013.12.027

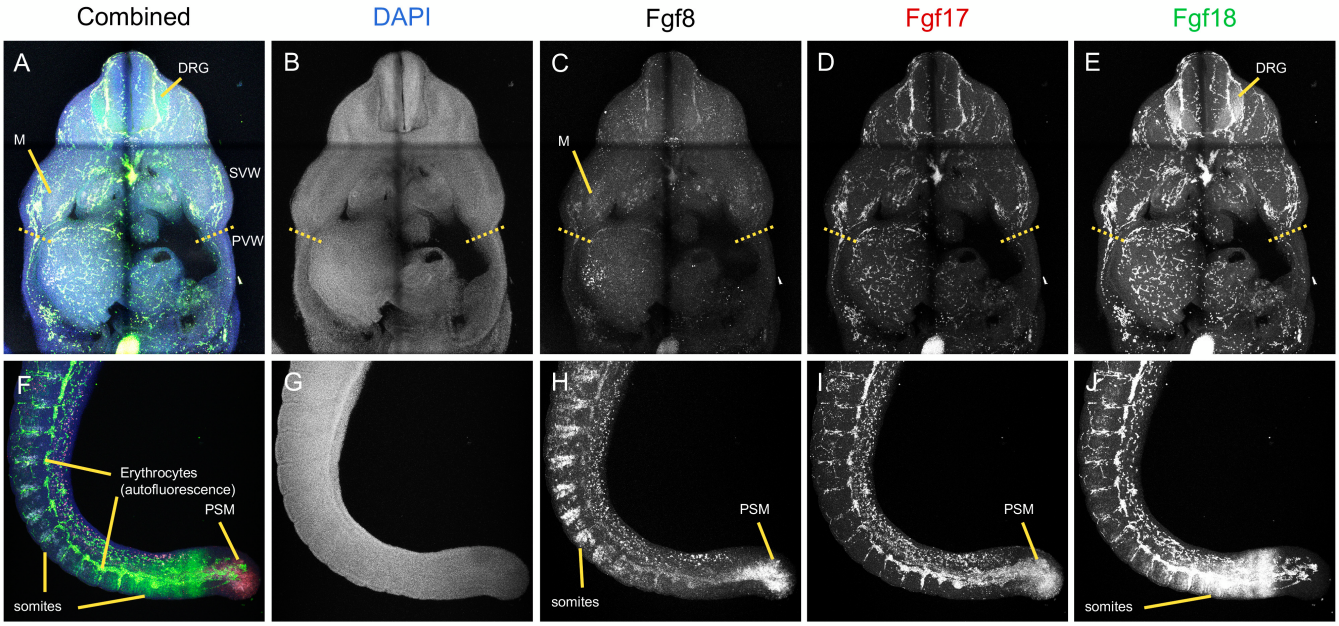

Figure S1. Expression of the *Fgf8* subfamily genes is undetectable in the E11.5 ventral body wall. Max intensity projection (MIP) of a Z-stack of E11.5 wildtype embryos stained for expression of *Fgf8*, *Fgf17* and *Fgf18* by hybridization chain reaction (Choi et al., 2018) . (A-E) Transverse image showing staining of DAPI (B), *Fgf8* (C), *Fgf17* (D), *Fgf18* (E). Note weak expression of *Fgf8* in the myotome (M) (A, C) and of *Fgf18* in the dorsal root ganglion (DRG) (A, E). There is no detectable expression of the Fgf8 subfamily genes in the secondary or primary ventral walls (separated by yellow dotted line in A–E). Lateral image of E11.5 tail showing previously established expression domains for *Fgf8* (H) *Fgf17* (I) and *Fgf18* (J) in somites and PSM. Note high autofluorescence of erythrocytes in all channels.

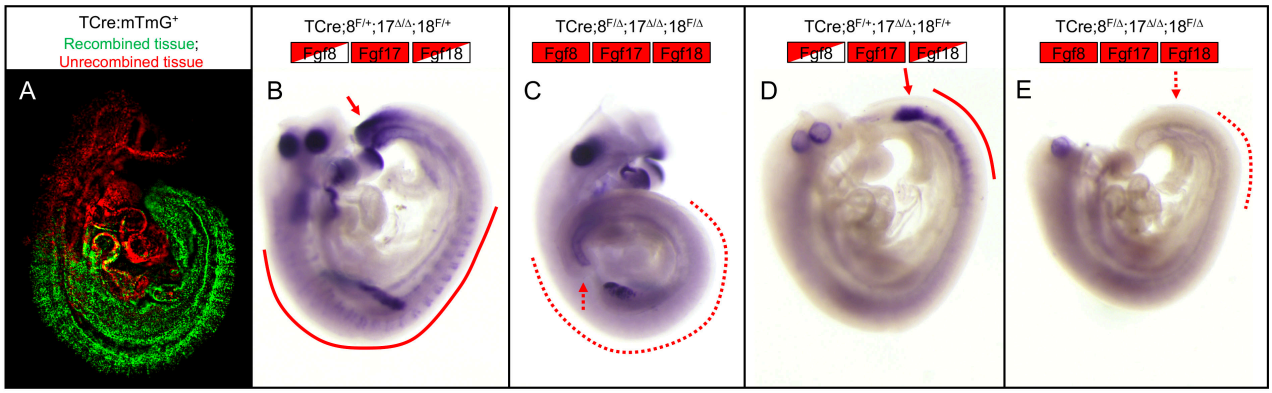

Figure S2. Characterization of TCre-mediated deletion of *Fgf8* and *Fgf18* (A) TCre; *mTmG* E9.5 embryo showing complete recombination in the PSM, the somites and LPM (green). (B,C) WISH using probe directed against the recombined region of *Fgf8* in E9.5 embryos. *Fgf8* transcript is detected as expected in the control embryo (B, arrow, PSM and line, somites) and is missing in the mutant embryo (C, dashed arrow and line). (D,E) WISH using probe directed against the recombined region of *Fgf18* in E9.5 embryos. *Fgf18* transcript is present as expected in control embryo (D, arrow, anterior PSM and line, somites) and is missing in the triple mutant embryo (E, dashed arrow and line). Boxes indicate genotype, see Fig. 2 for key.

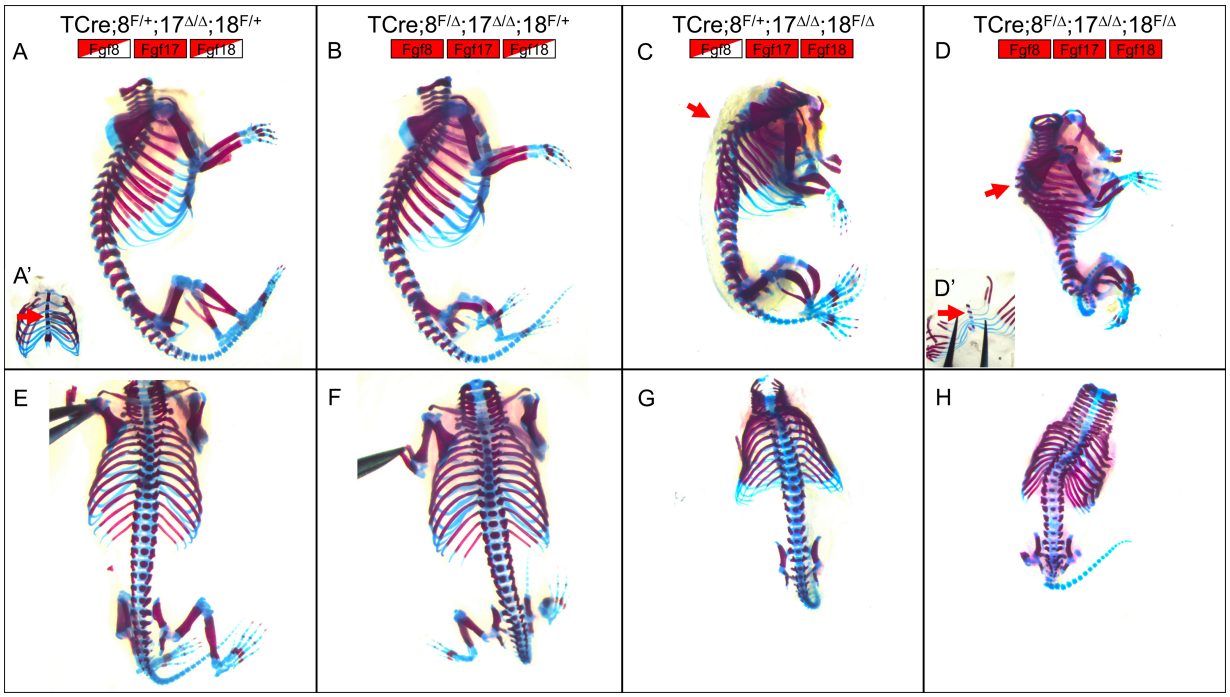

Figure S3. Loss of *Fgf8* and *Fgf17* exacerbates the skeletal defects seen in *Fgf18* loss-of-function embryos embryos at E18.5. (A-H) Alcian blue and alizarin red staining of skeletons of control (A,E), TCre;*Fgf8*$^{f/\Delta}$,*17*$^{\Delta/\Delta}$,*18*$^{f/+}$ (B,F); TCre;*Fgf8*$^{f/+}$,*17*$^{\Delta/\Delta}$,*18*$^{f/\Delta}$ (C,G) and triple mutant (D,H) embryos. Inserts A' and D' are ventral views of the indicated genotype showing correct sternum fusion (red arrows). E,F,G and H are a dorsal view of the same embryo in A,B,C and D, respectively. Note the kyphosis in C and D (arrow). Boxes indicate genotype, see Fig. 2 for key.

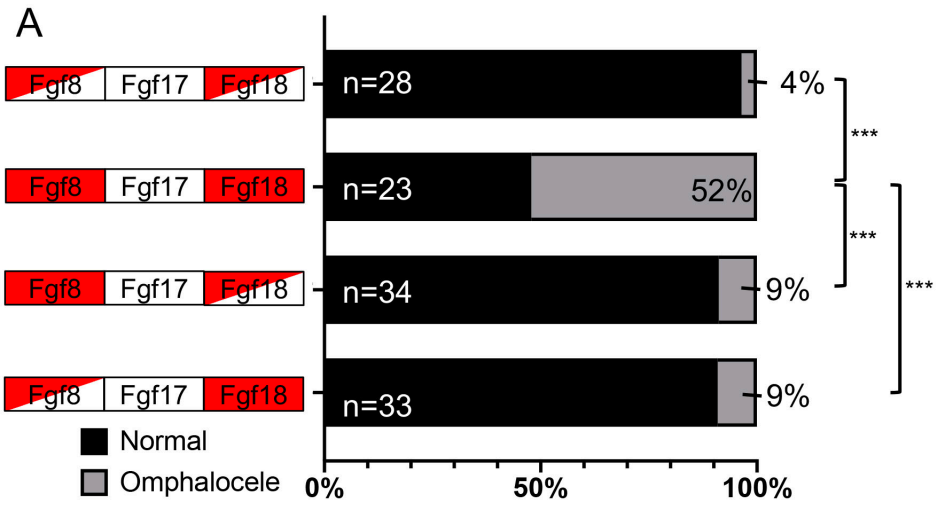

Figure S4. *Fgf17* does not rescue the omphalocele phenotype when copies of both *Fgf8* and *Fgf18* are inactivated. (A) Graphical representation of the incidence of omphalocele showing the percentage of embryos with and without omphalocele at E18.5. The total number of embryos is to the left of the bars and the percentage of embryos with omphalocele is on the right. Significance was found using a two-tailed Fisher's exact test. Boxes indicate genotype, see Fig. 2 for key.

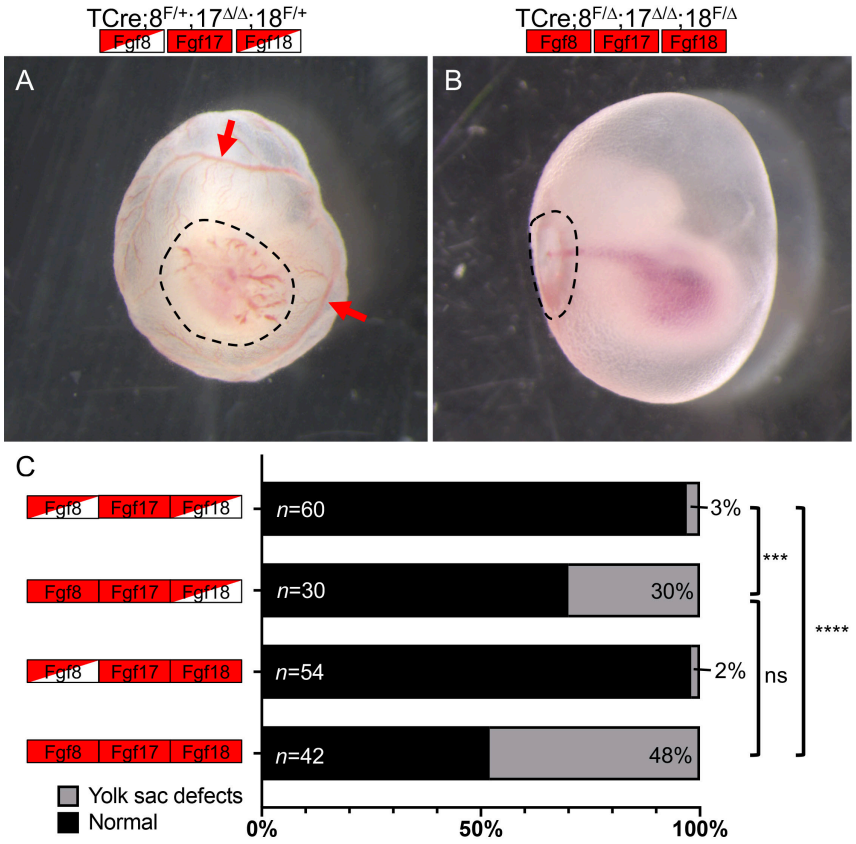

Figure S5. Loss of *Fgf8* results in an increased rate of yolk sac defects at E10.5. (A, B) E10.5 control (A) and triple mutant (B) embryo within the yolk sac. Mature yolk sac blood vessels indicated by arrows in A. Site of attachment to the chorion is indicated by a dashed circle. (C) Graphical representation of yolk sac defect incidence showing the percentage of embryos with and without yolk sac defects at E10.5, as determined by defective yolk sac remodeling and poor chorioallantoic fusion. The total number of embryos is to the left of the bars and the percentage of embryos with omphalocele is on the right. Significance was determined using a two-tailed Fisher's exact test. Boxes indicate genotype, see Fig. 2 for key.

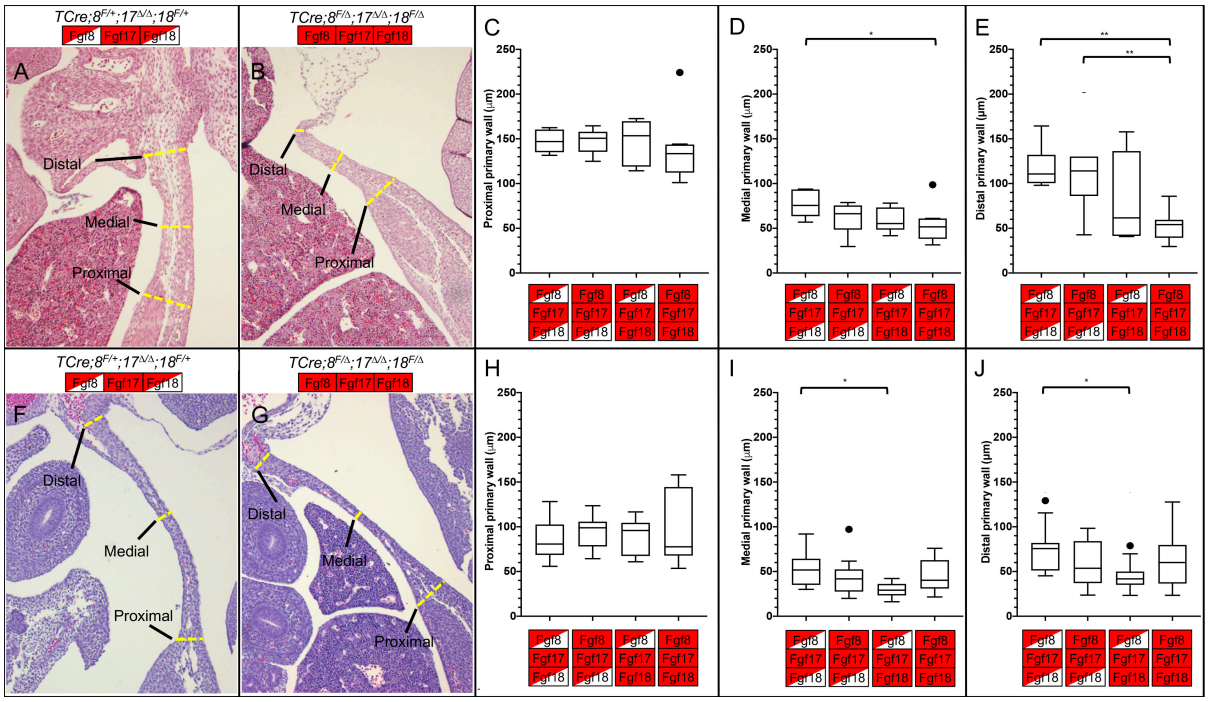

Figure S6. Morphometric analysis of sections at E13.5 and E12.5 reveals changes in the primary VW of *Fgf8* subfamily mutants. (A, B) Transverse section of E13.5 control (A) and triple mutant (B) at the interlimb region. (C-E) Tukey box-plots of the thickness of the E13.5 primary VW at the indicated positions (shown in A,B): proximal (C); medial (D); distal (E). Control *n*= 8; TCre;*Fgf8*$^{f/\Delta}$,*17*$^{\Delta/\Delta}$,*18*$^{f/+}$ *n*=7; TCre;*Fgf8*$^{f/+}$,*17*$^{\Delta/\Delta}$,*18*$^{f/\Delta}$ *n*=8; triple mutant *n*=9 (F,G) Transverse section of E12.5 control (F) and triple mutant (G) at the interlimb region. (H-I) Tukey box plots of the thickness of the E12.5 primary VW at the at the indicated positions (shown in F ,G): proximal proximal (H), medial (I) and distal (J) positions. Control *n*= 12; TCre;*Fgf8*$^{f/\Delta}$,*17*$^{\Delta/\Delta}$,*18*$^{f/+}$ *n*=10; TCre;*Fgf8*$^{f/+}$,*17*$^{\Delta/\Delta}$,*18*$^{f/\Delta}$ *n*=11; triple mutant *n*=11. Outliers in box-plots are plotted individually. Significance was found using a post-hoc Tukey-Kramer test. Boxes indicate genotype, see Fig. 2 for key.

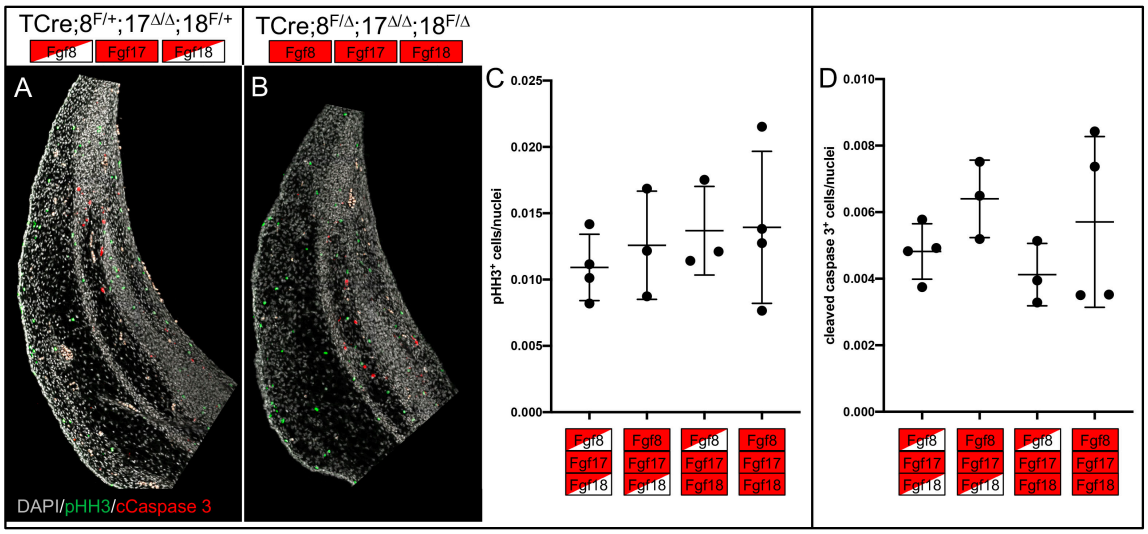

Figure S7. Cell proliferation and cell death in the secondary VW are unchanged in *Fgf8* subfamily mutants. (A,B) Max projection of 5 z-stacks from control (A) and triple mutant (B) transverse sections of the Secondary VW labelled with anti-pHH3 (green), anti-cleaved caspase 3 (red) and DAPI (white). (C) Ratio of pHH3 labelled cells to total nuclei. (D) Ratio of cleaved-caspase 3 to total nuclei. In C and D, data are plotted individually, mean±s.d. shown, a post-hoc Tukey-Kramer test applied. Control *n*=4; TCre;*Fgf8*$^{f/\Delta}$,*17*$^{\Delta/\Delta}$,*18*$^{f/+}$ *n*=3; TCre;*Fgf8*$^{f/+}$,*17*$^{\Delta/\Delta}$,*18*$^{f/\Delta}$ *n*=3; triple mutant *n*=4. Boxes indicate genotype, see Fig. 2 for key.

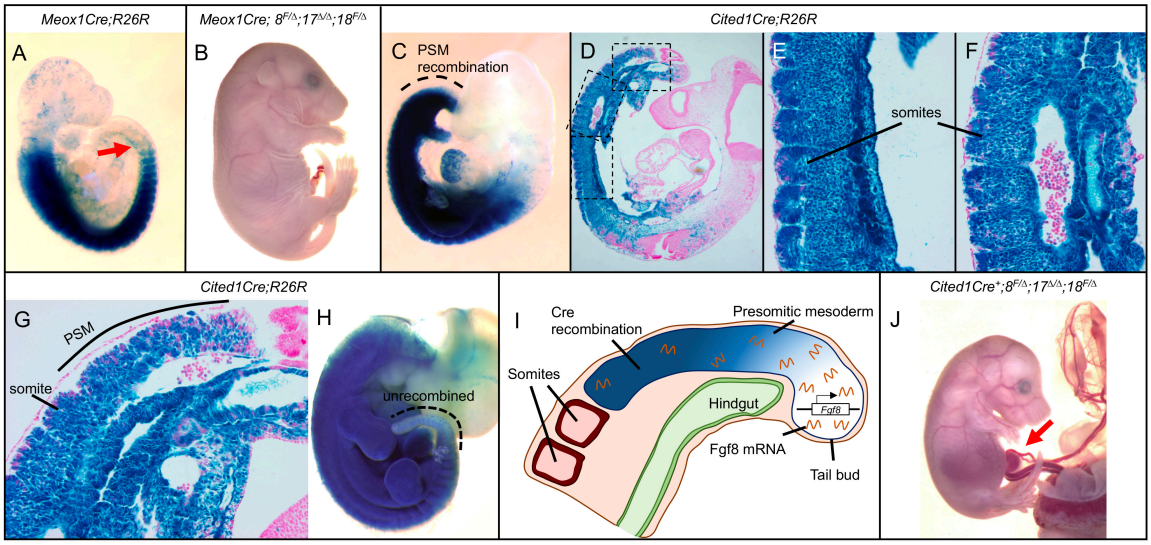

Figure S8. Meox1Cre recombines in the somites and Cited1Cre recombines in the PSM and the somites. (A) Recombination pattern of *Meox1Cre;R26R* E9.5 embryo, showing progressive somitic recombination (caudal-most somite indicated with arrow). (B) E18.5 *Meox1Cre;Fgf8*$^{f/\Delta}$*;Fgf17*$^{\Delta/\Delta}$*;Fgf18*$^{f/\Delta}$ embryo. (C-H) Recombination pattern of Cited1Cre*;R26R*, tamoxifen injected at E7.5 and E8.5. (see Materials and Methods). (C) Recombination pattern of E9.5 Cited1Cre*;R26R*, embryo. D) Sagittal section of *Cited1Cre;R26R*, with higher magnifications of boxed regions shown in E-G. (H) Recombination pattern of E11.5 Cited1Cre*;R26R*, embryo. (I) Diagram showing the mechanism of perdurance of *Fgf8* mRNA in the PSM in Cited1Cre*;Fgf8*$^{f/\Delta}$*;Fgf17*$^{\Delta/\Delta}$*;Fgf18*$^{f/+}$ and Cited1Cre;*Fgf8*$^{f/\Delta}$*;Fgf17*$^{\Delta/\Delta}$*;Fgf18*$^{f/\Delta}$ embryos. (J) E15.5 Cited1Cre triple mutant embryo, showing omphalocele (arrow).

Table S1. Genotypes of experimental crosses used in this study.

Experimental cross			Experimental genotype*	Frequency	Control genotypes*	Frequency
Fgf8$^{F/F}$;17$^{\Delta/\Delta}$;18$^{F/F}$	X	TCre$^{Tg/Tg}$;Fgf8$^{\Delta/+}$;17$^{\Delta/\Delta}$;18$^{\Delta/+}$	TCre;Fgf8$^{F/\Delta}$;17$^{\Delta/\Delta}$;18$^{F/\Delta}$	1:4	**TCre;Fgf8$^{F/+}$;17$^{\Delta/\Delta}$;18$^{F/+}$** TCre;Fgf8$^{F/\Delta}$;17$^{\Delta/\Delta}$;18$^{F/+}$ TCre;Fgf8$^{F/+}$;17$^{\Delta/\Delta}$;18$^{F/\Delta}$	1:4
Fgf8$^{F/F}$;17$^{+/+}$;18$^{F/F}$	X	TCre$^{Tg/Tg}$;Fgf8$^{\Delta/+}$;17$^{+/+}$;18$^{\Delta/+}$	TCre;Fgf8$^{F/\Delta}$;17$^{+/+}$;18$^{F/\Delta}$	1:4	**TCre;Fgf8$^{F/+}$;17$^{+/+}$;18$^{F/+}$** TCre;Fgf8$^{F/\Delta}$;17$^{+/+}$;18$^{F/+}$ TCre;Fgf8$^{F/+}$;17$^{+/+}$;18$^{F/\Delta}$	1:4
Fgf8$^{F/F}$;17$^{\Delta/\Delta}$;18$^{+/+}$	X	TCre$^{Tg/Tg}$;Fgf8$^{\Delta/+}$;17$^{\Delta/\Delta}$;18$^{+/+}$	TCre;Fgf8$^{F/\Delta}$;17$^{\Delta/\Delta}$;18$^{+/+}$	1:2	**TCre;Fgf8$^{F/+}$;17$^{\Delta/\Delta}$;18$^{+/+}$**	1:2
Fgf8$^{+/+}$;17$^{\Delta/\Delta}$;18$^{F/F}$	X	TCre$^{Tg/Tg}$;Fgf8$^{+/+}$;17$^{\Delta/\Delta}$;18$^{\Delta/+}$	TCre;Fgf8$^{+/+}$;17$^{\Delta/\Delta}$;18$^{F/\Delta}$	1:2	**TCre;Fgf8$^{+/+}$;17$^{\Delta/\Delta}$;18$^{F/+}$**	1:2
Fgf8$^{F/F}$;17$^{+/+}$;18$^{+/+}$	X	TCre$^{Tg/Tg}$;Fgf8$^{\Delta/+}$; 17$^{+/+}$;18$^{+/+}$	TCre;Fgf8$^{F/\Delta}$; 17$^{+/+}$;18$^{+/+}$	1:2	**TCre;Fgf8$^{F/+}$; 17$^{+/+}$;18$^{+/+}$**	1:2
Fgf8$^{+/+}$;17$^{\Delta/\Delta}$;18$^{+/+}$	X	TCre$^{Tg/Tg}$;Fgf8$^{+/+}$; 17$^{\Delta/\Delta}$;18$^{+/+}$	TCre;Fgf8$^{+/+}$; 17$^{\Delta/\Delta}$;18$^{+/+}$	1	**N/A**	N/A
Fgf8$^{+/+}$;17$^{+/+}$;18$^{F/F}$	X	TCre$^{Tg/Tg}$;Fgf8$^{+/+}$;17$^{+/+}$;18$^{\Delta/+}$	TCre;Fgf8$^{+/+}$;17$^{+/+}$;18$^{F/\Delta}$	1:2	**TCre;Fgf8$^{+/+}$;17$^{+/+}$;18$^{F/+}$**	1:2
Fgf8$^{F/F}$;17$^{\Delta/\Delta}$;18$^{F/F}$	X	Cited1Cre^{Tg};Fgf8$^{\Delta/+}$;17$^{\Delta/\Delta}$;18$^{\Delta/+}$	Cited1Cre;Fgf8$^{F/\Delta}$;17$^{\Delta/\Delta}$;18$^{F/\Delta}$	1:8	**Cited1Cre;Fgf8$^{F/+}$;17$^{\Delta/\Delta}$;18$^{F/+}$** Cited1Cre;Fgf8$^{F/\Delta}$;17$^{\Delta/\Delta}$;18$^{F/+}$ Cited1Cre;Fgf8$^{F/+}$;17$^{\Delta/\Delta}$;18$^{F/\Delta}$	1:8
Fgf8$^{F/F}$;17$^{\Delta/\Delta}$;18$^{F/F}$	X	Meox1$^{Cre/+}$;Fgf8$^{\Delta/+}$;17$^{\Delta/\Delta}$;18$^{\Delta/+}$	Meox1$^{Cre/+}$;Fgf8$^{F/\Delta}$;17$^{\Delta/\Delta}$;18$^{F/\Delta}$	1:8	**Meox1$^{Cre/+}$;Fgf8$^{F/+}$;17$^{\Delta/\Delta}$;18$^{F/+}$** Meox1$^{Cre/+}$;Fgf8$^{F/\Delta}$;17$^{\Delta/\Delta}$;18$^{F/+}$ Meox1$^{Cre/+}$;Fgf8$^{F/+}$;17$^{\Delta/\Delta}$;18$^{F/\Delta}$	1:8

The experimental cross is always written 'female x male'.
Δ, 'deletion' or null; +, wild-type.
The most wild-type control from a genetic cross is written in bold.
The genotypes of Cre-negative offspring from crosses using Meox1Cre and Cited1Cre are not shown here.